A MULTIFACETED APPROACH TO IDENTIFYING TARGETS FOR THE IMPROVEMENT OF WATER-USE EFFICIENCY IN *ZEA MAYS*

BY

ROBERT JAMES TWOHEY III

THESIS

Submitted in partial fulfillment of the requirements
for the degree of Master of Science in Crop Sciences
in the Graduate College of the
University of Illinois at Urbana-Champaign, 2019

Urbana, Illinois

Master's Committee:

Assistant Professor Anthony J. Studer, Chair
Professor Andrew Leakey
Assistant Professor Martin Sachs

ABSTRACT

Current climate projections and the need for sustainability require the development of more efficient crops. With fresh water resources declining and precipitation patterns becoming more sporadic, severe drought scenarios are becoming a normal occurrence during production seasons. Current methods for quantifying water-use efficiency (WUE) in C_4 crops are not able to screen large quantities of lines. Stable carbon isotope composition ($\delta^{13}C$) has been successfully used to breed for higher WUE in C_3 crops. This has not been the case in C_4 species due to their more complex photosynthetic mechanism. We present data demonstrating that leaf $\delta^{13}C$ variation exists across lines of *Z. mays*, and is a heritable trait. Appropriate and optimal leaf $\delta^{13}C$ sample collection was determined through developmental and circadian time courses as a means to standardize the use of $\delta^{13}C$ as a proxy trait for transpiration efficiency. In addition, the relationship between $\delta^{13}C$ and transpiration was established. The use of leaf $\delta^{13}C$ has the potential to be used as a breeding tool to increase the transpiration efficiency and WUE of maize.

Atmospheric CO_2 has increased over the past decade and projections show greater increases in the future. Understanding how stomata will respond to high atmospheric CO_2 concentrations and accompanying environmental changes is necessary for the production of efficient crops. Stomata are the major avenue for CO_2 uptake and also the avenue for transpirational water loss. As a result, a balance between CO_2 integration and water loss is important for desirable photosynthetic rates while maintaining a healthy plant water status. The CO_2 stomatal signaling pathway was previously elucidated in the dicot species *A. thaliana*. We characterized orthologs believed to hold importance in the *Z. mays* CO_2 signaling pathway using genetic mutants and gas exchange physiology. By identifying the mechanisms stomata use to respond to varying CO_2 levels in *Z. mays*, we can begin to engineer stomatal dynamics to produce an efficient crop under changing climates.

ACKNOWLEDGEMENTS

First, I would like to thank my advisor, Dr. Anthony J. Studer. His excellent guidance and thoughtful input since day one made this work possible. He has greatly strengthened my research capabilities by training me how to conduct experimental design, execution of our research projects, and the important task of analyzing and composing results for publication. I would also like to thank my committee members Dr. Andrew Leakey and Dr. Marty Sachs for their valuable input and guidance during my Masters research.

I would like to thank all my lab mates who have helped in any part with my research. I thank Lucas Roberts especially for the collaboration on our stable carbon isotope work. Without the teamwork of our lab, the research completed would not have been accomplished. I also would like to thank the PCF greenhouse staff and the Research farm staff, as we would not have our research crops without them.

I owe many thanks to my family for the support they have given me. My parents and brothers have always encouraged and driven me to accomplish what I set out to do.

Finally, I thank Bailee for all the times she has helped me during my Master's degree. She has supported and pushed me to continue what I enjoy.

TABLE OF CONTENTS

CHAPTER 1

Introduction

Increases in atmospheric CO_2 concentrations have been observed over the previous decades, and are projected to continue in the future. Current atmospheric CO_2 concentrations are above 400 ppm, and have risen around 25 ppm annually since 2008 (Shaftel et al., 2019). The main contributors driving the drastic increase in atmospheric CO_2 are the burning of fossil fuels and the release of carbon sources during land development and clearing (Raupach et al., 2007). CO_2 acts as the primary carbon source for plant metabolism necessary to support life on earth. Atmospheric CO_2 is also a signaling molecule that regulates fundamental processes related to plant growth and development. The rise in atmospheric CO_2 is causing a variety of changes at a global scale. Given the magnitude of these changes, there is a need to better understand how crops will respond to changing environmental factors to ensure food security in future climates.

By 2080, global temperature is projected to increase by as much as 4.7°C (US global change 2019). A rise in temperature will cause an increase in the water holding capacity of the air, which causes an increase in evapotranspiration (Long and Ort, 2010). Greater evapotranspiration will increase the demand for soil moisture and lead to quicker depletion of surface moisture that is critical for sustaining agricultural production. Additionally, rainfall patterns are becoming more sporadic and less frequent with a majority of our yearly rain totals falling during heavy rain events. The combination of these changes will lead to more frequent and longer periods of drought (Lobell et al., 2014). Variability in precipitation will likely negatively impact crop yields, especially in rainfed areas (Pendergrass et al., 2017). Since less than a quarter of the production acres in the United States are irrigated, these environmental changes could be seriously damaging (NASS 2013). Agricultural irrigation is already the largest user of fresh water reserves, while only 2.5% of earth's water is considered fresh (USDA, 2017, Gleick, 1993). Therefore, in response to changing climate conditions it is necessary to identify and implement strategies to optimize water use in major crops.

In the US alone, 89.1 million acres of *Zea mays* was planted in 2018 (NASS 2019), and each acre is calculated to transpire 3,000 to 4,000 gallons of water per day (Leopold, 1960). These statistics highlight the scale of modern agriculture, and the impact it can have on limited natural resources such as fresh water. When thinking about improving crop water relations, it is

important to understand the differences between water-use efficiency (WUE) and drought tolerance. Plants considered to have a high drought tolerance are able to survive prolonged periods with little to no available water in the surrounding soil. Plants that have a high WUE can employ several different mechanisms for conserving water resources. Water use efficient plants preserve water reserves under well-watered conditions, making it available during periods of drought. Two commonly used methods of measuring WUE are agronomic transpiration efficiency TE_a and intrinsic transpiration efficiency TE_{leaf}. To calculate TE_a, a ratio between aboveground biomass and the total amount of water used is determined (Codon et al., 2004). To determine TE_{leaf} values, the ratio of net photosynthesis (*A*) and transpiration (*E)* is calculated (Codon et al., 2002). Currently, TE_a can be determined by weighing pots in greenhouse experiments and TE_{leaf} using gas exchange measurements. These methods are successful at quantifying TE, however are not able to scale to a breeding level due to the amount of resources and time required for data collection. Therefore, high throughput methods for quantifying TE at a field scale remains unidentified. New methods to quantify TE in major crops would be beneficial to breeding programs, especially for developing climate resiliency.

Assaying stable carbon isotope composition has been successfully used to breed water-use efficient C_3 crops, but not in C_4 crops (von Caemmerer et al., 2014). There are two stable carbon isotopes naturally present on earth. The ^{12}C isotope is the most abundant (98.9%) with the remaining as ^{13}C (1.1%) (Farquhar et al., 1989). During the uptake and fixation of CO_2 by plants, ^{12}C and ^{13}C are discriminated against at varying levels depending on the fractionation step (Caemmerer et al., 2014). Discrimination occurs due to kinetic effects as ^{13}C is a heavier isotope compared to ^{12}C. As a result, $^{13}C/^{12}C$ ratios can report information about internal plant processes responsible for fixation of CO_2 (Farquhar et al., 1989). Carbon isotope composition ($\delta^{13}C$) is a relativized value comprised of the plant tissue sample $^{13}C/^{12}C$ ratio relative to the $^{13}C/^{12}C$ ratio of the international standard, limestone Pee Dee belemnite (Codon et al., 2002).

$$\delta^{13}C = \left[\frac{R_{sample}}{R_{standard}} - 1\right] \times 1000$$

In C_3 species, CO_2 moves through stomata into the intercellular air space. A small amount of fractionation occurs during diffusion to the site of carboxylation. Then, carboxylation by Rubisco occurs in mesophyll cells, which is the largest fractionation event (O'Leary, 1988). All of the

fractionation steps in C_3 species discriminate against ^{13}C. Fractionation and the resulting $^{13}C/^{12}C$ ratio is different in C_4 species. The initial fractionation event is diffusion to the site of carbonic anhydrase (CA) hydration, discriminating against ^{13}C. Next, the production of bicarbonate (HCO_3^-) by CA discriminates against ^{12}C, concentrating ^{13}C. Then, HCO_3^- is taken up by phosphoenolpyruvate carboxylase (PEPC) where ^{13}C is discriminated against. During these two fractionation events, there is an overall net discrimination against ^{12}C occurring. A large fractionation event then occurs when CO_2 is used by Rubisco, but this fractionation does not greatly influence the $\delta^{13}C$ values because the initial fractionation by CA/PEPC is irreversible. Overall, the steps in C_4 plants, shown to be significant in isotopic fractionation, are diffusion through stomata and the ^{12}C discrimination by CA (O'leary, 1988). Interestingly, Kolbe et al. did not find any relationship between enzyme activity and $\delta^{13}C$ (2018). This means that $\delta^{13}C$ variation is likely driven by factors other than fractionation events, such as bundle sheath leakiness or g_s.

Due to the connection between carbon isotope composition and stomatal aperture, $\delta^{13}C$ has been used as a proxy trait for TE in C_3 plants (Impa et al., 2015; Farquhar and Richards, 1984; Ehdaie et al., 1991). However, this technique has not yet been fully established in C_4 species because of the more complex relationship between $\delta^{13}C$ and TE (Gresset et al., 2014; Ellsworth et al., 2019). In *Sorghum bicolor,* genetic and environmental variation in isotopic values have been observed (Henderson et al., 1998). However, the relationship between carbon isotopes and TE in *S. bicolor* has not been fully unraveled due to significant variation observed in carbon isotope values across varying environments. Therefore, carbon isotopes are currently not being used to identify *S. bicolor* lines with high TE. In Chapter 2, we further investigate the relationship between TE and $\delta^{13}C$ in *Z. mays* and determine optimal sample times of leaf tissue $\delta^{13}C$. Using $\delta^{13}C$ as a tool will allow us to identify physiological processes that can contribute to increasing WUE in C_4 crops.

Stomatal pores present on the leaf surface are critical for modulating photosynthesis and transpiration. Stomata respond to a number of environmental factors such as humidity, temperature, light intensity, and atmospheric CO_2 concentrations (Grantz, 1990; Schulze et al., 1973; Kinoshita et al., 2001; Kolbe et al., 2019). Stomata are composed of two guard cells surrounded by epidermal and subsidiary cells. Each pair of guard cells open and close to regulate the influx of CO_2 and the efflux of water vapor. The turgor pressure of each guard cell is altered

to produce a turgid or flaccid cell resulting in opening or closing, respectively. Rates of CO_2 and water exchange between the atmosphere and leaf increase with the opening of stomata (Hetherington, 2001).

The signaling pathway responsible for stomatal response to changes in atmospheric CO_2 concentration has been mostly studied in dicots (Tian et al., 2015; Hsu et al., 2018; Kim et al., 2010). Through mutant analysis, a biochemical pathway was constructed in *Arabidopsis thaliana*. As CO_2 crosses the plasma membrane, it is aided by plasma membrane intrinsic proteins (PIPs). The PIPs are passive transporters, some being permeable to CO_2 and water. Although *PIP1;2* has been shown to associate with downstream components of the CO_2 stomatal signaling pathway, a T-DNA insertion mutant exposed to changing atmospheric CO_2 levels showed a similar stomatal responses to wild type (WT) plants (Wang et al., 2016). The presence of multiple aquaporin genes with redundant function is likely the cause for WT like responses in the *PIP1;2* mutant. Once CO_2 enters the guard cells, carbonic anhydrase (CA) catalyzes the hydration of CO_2 to bicarbonate (HCO_3^-). A *ca1ca4* double mutant resulted in stomatal insensitivity to altered CO_2 concentrations (Hu et al., 2010). Resistant to High CO_2 1 (RHC1) was identified as a bicarbonate sensor and characterization of a stably transformed *rhc1* T-DNA exon insertion mutant showed a lack of stomatal response to increasing CO_2 levels (Tian et al., 2015). In this same study, a RHC1 compliment restored stomatal response comparable to WT plants. Activation of RHC1 by HCO_3^- accumulation results in the binding of RHC1 to High Leaf Temperature 1 (HT1) (Tian et al., 2015). Characterization of two mutant alleles of the gene HT1 (*ht1-1* and *ht1-2*) showed insensitivity in stomatal response to changes in atmospheric CO_2 levels compared to WT plants (Hashimoto et al., 2006). The binding of RHC1 and HT1 prevents the inhibition of protein kinases by HT1. Currently, Open Stomata 1 (OST1) and Guard Cell Hydrogen Peroxide-Resistant1 (GHR1) are known kinases functioning in this signaling pathway (Matrosova et al., 2015; Hõrak et al., 2016). Mutant alleles of OST1 and GHR1 have been shown to disrupt stomatal signaling in response to CO_2 and ABA changes (Xue et al. 2011; Hõrak et al., 2016). As the final step of the pathway, Slow Anion Channel-Associated 1 (SLAC1) is activated by a protein kinase. SLAC1 is an S-type anion channel that pumps chloride out of the guard cells, resulting in stomatal closure. Mutations of SLAC1 produced extreme insensitivities to changes in atmospheric CO_2 levels (Vahisalu et al., 2008; Negi et al., 2008).

With this information and the use of double mutant analysis, a near complete signaling pathway has been elucidated in *A. thaliana.*

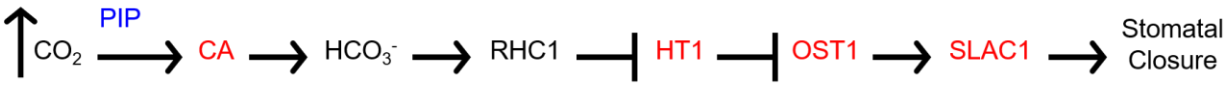

Previous findings in *A. thaliana* have been a valuable resource to better understand the mechanisms and signaling cascades responsible for stomatal response to environmental factors. It has provided us with an initial framework to investigate CO_2 concentration and stomatal interactions in monocots. As many of our major crops are monocots, in Chapter 3 we further investigated the similarities and differences in stomatal signaling between monocots and dicots using the C_4 grass *Z. mays*. A greater understanding of the CO_2 signaling pathway in *Z. mays* will facilitate future improvement in stomatal response to changing CO_2 levels and possibly TE. Stomata are not always efficient at responding to environmental changes. Stomatal movements could be up to an order of magnitude slower in response to environmental changes compared to photosynthetic responses, and stomatal overshooting frequently occurs (Lawson and Blatt, 2014; Raschke and Kühl, 1969). Because of these slow responses, unnecessary water loss and loss of photosynthetic efficiency can occur (Hines, 2019). Modifying the genetic regulation of signaling pathways or a reduction in stomatal number could improve stomatal response efficiency and TE (Bertolino et al., 2019). Elucidating the CO_2 stomatal signaling pathway in *Z. mays* would allow us to engineer stomatal dynamics to produce an efficient crop under changing environmental conditions in the future.

Given global climate predictions of increases in temperature, drought severity, and CO_2 levels, methods for optimizing stomatal response and WUE in our major crops is essential. It has been shown that WUE is a complex trait, however advancements provide evidence that WUE can be improved in crop species (Leakey et al., 2019). Two methods for optimizing crop water relations have been targeted. First, a greater understanding of the relationship between $\delta^{13}C$ and TE in C_4 species could lead to breeding methods that can be utilized to select for more WUE crops. Second, the investigation and elucidation of the CO_2 stomatal signaling pathway in Z. mays could allow for targeted control of stomatal dynamics. The following two chapters represent our work in these areas and lay the foundation for future studies.

REFERENCES

Bertolino, L. T., Caine, R. S., & Gray, J. E. (2019). Impact of stomatal density and morphology on water-use efficiency in a changing world. *Frontiers in plant science*, *10*.

Condon, A. G., Richards, R. A., Rebetzke, G. J., & Farquhar, G. D. (2002). Improving intrinsic water-use efficiency and crop yield. *Crop science*, *42*(1), 122-131.

Condon, A. G., Richards, R. A., Rebetzke, G. J., & Farquhar, G. D. (2004). Breeding for high water-use efficiency. *Journal of experimental botany*, *55*(407), 2447-2460.

Ehdaie, B., Hall, A. E., Farquhar, G. D., Nguyen, H. T., & Waines, J. G. (1991). Water-use efficiency and carbon isotope discrimination in wheat. *Crop science*, *31*(5), 1282-1288.

Ellsworth, P., Feldman, M., Baxter, I., & Cousins, A. (2019). A genetic link between leaf carbon isotope composition and whole-plant water use efficiency in the C_4 grass Setaria. *BioRxiv*, 285676.

Farquhar, G. D., Ehleringer, J. R., & Hubick, K. T. (1989). Carbon isotope discrimination and photosynthesis. *Annual review of plant biology*, *40*(1), 503-537.

Farquhar, G. D., & Richards, R. A. (1984). Isotopic composition of plant carbon correlates with water-use efficiency of wheat genotypes. *Functional Plant Biology*, *11*(6), 539-552.

Gleick, P. H. (1993). Water and conflict: Fresh water resources and international security. *International security*, *18*(1), 79-112.

Grantz, D. A. (1990). Plant response to atmospheric humidity. *Plant, Cell & Environment*, *13*(7), 667-679.

Gresset, S., Westermeier, P., Rademacher, S., Ouzunova, M., Presterl, T., Westhoff, P., & Schön, C. C. (2014). Stable carbon isotope discrimination is under genetic control in the C_4 species maize with several genomic regions influencing trait expression. *Plant Physiology*, *164*(1), 131-143.

Henderson, S., Von Caemmerer, S., Farquhar, G. D., Wade, L., & Hammer, G. (1998). Correlation between carbon isotope discrimination and transpiration efficiency in lines of

the C4 species Sorghum bicolor in the glasshouse and the field. *Functional Plant Biology*, *25*(1), 111-123.

Hetherington, A. M. (2001). Guard cell signaling. Cell, 107(6), 711-714.

Lawson, T., & Blatt, M. R. (2014). Stomatal size, speed, and responsiveness impact on photosynthesis and water use efficiency. *Plant physiology*, *164*(4), 1556-1570.

Leakey, A. D., Ferguson, J. N., Pignon, C. P., Wu, A., Jin, Z., Hammer, G. L., & Lobell, D. B. (2019). Water use efficiency as a constraint and target for improving the resilience and productivity of C3 and C4 crops. *Annual review of plant biology*, *70*, 781-808.

O'Leary, M. H. (1988). Carbon isotopes in photosynthesis. *Bioscience*, *38*(5), 328-336.

Hashimoto, M., Negi, J., Young, J., Israelsson, M., Schroeder, J. I., & Iba, K. (2006). Arabidopsis HT1 kinase controls stomatal movements in response to CO_2. *Nature cell biology*, *8*(4), 391.

Hines, P. J. (2019). Speeding up stomatal responses.

Hsu, P. K., Takahashi, Y., Munemasa, S., Merilo, E., Laanemets, K., Waadt, R., Pater, D., Kollist, H., & Schroeder, J. I. (2018). Abscisic acid-independent stomatal CO_2 signal transduction pathway and convergence of CO_2 and ABA signaling downstream of OST1 kinase. *Proceedings of the National Academy of Sciences*, *115*(42), E9971-E9980.

Hu, H., Boisson-Dernier, A., Israelsson-Nordström, M., Böhmer, M., Xue, S., Ries, A., Godoski, J., Kuhn, J. M., & Schroeder, J. I. (2010). Carbonic anhydrases are upstream regulators of CO_2-controlled stomatal movements in guard cells. *Nature cell biology*, *12*(1), 87.

Impa, S. M., Nadaradjan, S., Boominathan, P., Shashidhar, G., Bindumadhava, H. Y., & Sheshshayee, M. S. (2005). Carbon isotope discrimination accurately reflects variability in WUE measured at a whole plant level in rice. *Crop Science*, *45*(6), 2517-2522.

Kim, T. H., Böhmer, M., Hu, H., Nishimura, N., & Schroeder, J. I. (2010). Guard cell signal transduction network: advances in understanding abscisic acid, CO_2, and Ca^{2+} signaling. *Annual review of plant biology*, *61*, 561-591.

Kinoshita, T., Doi, M., Suetsugu, N., Kagawa, T., Wada, M., & Shimazaki, K. I. (2001). Phot1 and phot2 mediate blue light regulation of stomatal opening. *Nature*, *414*(6864), 656.

Kolbe, A. R., Studer, A. J., Cornejo, O. E., & Cousins, A. B. (2019). Insights from transcriptome profiling on the non-photosynthetic and stomatal signaling response of maize carbonic anhydrase mutants to low CO_2. *BMC genomics*, *20*(1), 138.

Kolbe, A. R., Studer, A. J., & Cousins, A. B. (2018). Biochemical and transcriptomic analysis of maize diversity to elucidate drivers of leaf carbon isotope composition. *Functional Plant Biology*, *45*(5), 489-500.

Leopold, L. B., & Langbein, W. B. (1960). *A primer on water*. US Government Printing Office.

Lobell, D. B., Roberts, M. J., Schlenker, W., Braun, N., Little, B. B., Rejesus, R. M., & Hammer, G. L. (2014). Greater sensitivity to drought accompanies maize yield increase in the US Midwest. *Science*, *344*(6183), 516-519.

Long, S.P., Ort, D.R. (2010). More than taking the heat: crops and global change. Current Opinion in Plant Biology, 13, 240-247.

Matrosova, A., Bogireddi, H., Mateo-Peñas, A., Hashimoto-Sugimoto, M., Iba, K., Schroeder, J. I., & Israelsson-Nordström, M. (2015). The HT1 protein kinase is essential for red light-induced

Negi, J., Matsuda, O., Nagasawa, T., Oba, Y., Takahashi, H., Kawai-Yamada, M., Uchimiya, H., Hashimoto, & M., Iba, K. (2008). CO_2 regulator SLAC1 and its homologues are essential for anion homeostasis in plant cells. *Nature*, *452*(7186), 483.

Pendergrass, A. G., Knutti, R., Lehner, F., Deser, C., & Sanderson, B. M. (2017). Precipitation variability increases in a warmer climate. *Scientific reports*, *7*(1), 17966.

Raschke, K., & Kühl, U. (1969). Stomatal responses to changes in atmospheric humidity and water supply: Experiments with leaf sections of *Zea mays* in CO_2-free air. *Planta*, *87*(1-2), 36-48.

Raupach, M. R., Marland, G., Ciais, P., Le Quéré, C., Canadell, J. G., Klepper, G., & Field, C. B. (2007). Global and regional drivers of accelerating CO_2 emissions. *Proceedings of the National Academy of Sciences*, *104*(24), 10288-10293.

Schulze, E. D., Lange, O. L., Kappen, L., Buschbom, U., & Evenari, M. (1973). Stomatal responses to changes in temperature at increasing water stress. *Planta*, *110*(1), 29-42.

Shaftel, H., Jackson, R., Callery, S. (2019). Global Climate Change: Vital Signs of the Planet. NASA's Jet Propulsion Laboratory. (https://climate.nasa.gov/)

Sheshshayee, M. S., Bindumadhava, H., Shankar, A. G., Prasad, T. G., & Udayakumar, M. (2003). Breeding strategies to exploit water use efficiency for crop improvement. *Journal of plant biology-New Delhi*, *30*(2), 253-268.

Tian, W., Hou, C., Ren, Z., Pan, Y., Jia, J., Zhang, H., Bai, F., Zhang, P., Zhu, H., He, Y., Luo, S., Li, L., Luan, S. (2015). A molecular pathway for CO 2 response in Arabidopsis guard cells. *Nature Communications*, *6*, 6057.

Vahisalu, T., Kollist, H., Wang, Y. F., Nishimura, N., Chan, W. Y., Valerio, G., Lamminmäki, A., Brosché, M., Moldau, H., Desikan, R., Schroeder, J. I., & Kangasjärvi, J. (2008). SLAC1 is required for plant guard cell S-type anion channel function in stomatal signaling. *Nature*, *452*(7186), 487.

von Caemmerer, S. V., Ghannoum, O., Pengelly, J. J., & Cousins, A. B. (2014). Carbon isotope discrimination as a tool to explore C4 photosynthesis. *Journal of experimental botany*, *65*(13), 3459-3470.

Wang, C., Hu, H., Qin, X., Zeise, B., Xu, D., Rappel, W. J., Boron, W. F., & Schroeder, J. I. (2016). Reconstitution of CO2 regulation of SLAC1 anion channel and function of CO2-permeable PIP2; 1 aquaporin as CARBONIC ANHYDRASE4 interactor. *The Plant Cell*, *28*(2), 568-582.

Xue, S., Hu, H., Ries, A., Merilo, E., Kollist, H., & Schroeder, J. I. (2011). Central functions of bicarbonate in S-type anion channel activation and OST1 protein kinase in CO_2 signal transduction in guard cell. *The EMBO journal*, *30*(8), 1645-1658.

CHAPTER 2

Leaf Stable Carbon Isotope Composition Reflects Transpiration Efficiency in *Zea mays**

ABSTRACT

The increasing demand for food production and predicted climate change scenarios highlight the need for improvements in crop sustainability. The efficient use of water will become increasingly important for rainfed agricultural crops even in fertile regions that have historically received ample precipitation. Improvements in water-use efficiency in *Zea mays* have been limited, and warrants a renewed effort aided by molecular breeding approaches. Progress has been constrained by the difficulty of measuring water-use in a field environment. The stable carbon isotope composition ($\delta^{13}C$) of the leaf has been proposed as an integrated signature of carbon fixation with a link to stomatal conductance. However, additional factors affecting leaf $\delta^{13}C$ exist, and a limited number of studies have explored this trait in *Z. mays*. Here we present an extensive characterization of leaf $\delta^{13}C$ in *Z. mays*. Significant variation in leaf $\delta^{13}C$ exists across diverse lines of *Z. mays*, which we show to be heritable across several environments. Furthermore, we examine temporal and spatial variation in leaf $\delta^{13}C$ to determine the optimum sampling time to maximize the use of leaf $\delta^{13}C$ as a trait. Finally, our results demonstrate the relationship between transpiration and leaf $\delta^{13}C$ in the field and the greenhouse. Decreasing transpiration and soil moisture are associated with decreasing leaf $\delta^{13}C$. Taken together these results outline a strategy for using leaf $\delta^{13}C$ and reveal its usefulness as a measure of transpiration efficiency under well-watered conditions rather than a predictor of performance under drought.

INTRODUCTION

Increasing occurrences of extreme temperature and precipitation patterns necessitate improvements in crop productivity and sustainability (Pryor *et al.*, 2013). In the near future,

---

*Published as:

Twohey III, R. J., Roberts, L. M., & Studer, A. J. (2019). Leaf stable carbon isotope composition reflects transpiration efficiency in Zea mays. *The Plant Journal, 97*(3), 475-484.

abnormal and sporadic precipitation in the Midwestern United States, where agriculture is primarily rainfed, will require crops that use water efficiently. The susceptibility of *Zea mays* to yield loss due to increases in temperature and vapor pressure deficit (VPD; the difference between the amount of water in the air and the holding capacity of the air when saturated) has already been documented in this region (Lobell *et al.*, 2014). An extensive amount of time is required to develop a commercial variety with improvements in complex traits that affect canopy dynamics, photosynthetic pathways, and water-use (Hall and Richards, 2013). Thus, advancements in methods for evaluating water use are required to speed up breeding efforts to meet the imminent need for more efficient and sustainable crops.

Transpiration efficiency can be defined in agronomic terms (TE_a = yield ÷ transpired water) or leaf level terms as (TE_{leaf} = net photosynthesis ÷ transpiration) (Dhanapal *et al.*, 2015; Ellsworth and Cousins, 2016). Transpiration is the efflux of water through stomatal pores that occurs simultaneously with the influx of CO_2 for photosynthesis (Kim *et al.*, 2010), and can be calculated by multiplying stomatal conductance (g_s) by VPD. Importantly, an increase in *TE* must not limit CO_2 for photosynthesis, which would result in a reduction in yield. This is problematic in a C_3 crop because high g_s, which equates to high transpiration, is generally required to maintain high levels of photosynthesis. In fact, high yielding C_3 crops have been shown to be associated with high g_s (reviewed in Blum, 2009). However, in C_4 crops, the carbon concentrating mechanism maintains high concentrations of CO_2 around Rubisco in the bundle sheath cells even when g_s is low (von Caemmerer, 2000). Therefore, in a C_4 crop, there is the potential to optimize *TE*.

Direct measurements of *TE* are both time and resource consuming. These constraints are compounded by the large population size needed for a breeding program (Long and Bernacchi, 2003), but there may be high-throughput alternatives to traditional gas exchange assays. One of the proposed alternative methods is the use of carbon isotope composition of a leaf ($\delta^{13}C$, *‰*) as an integrative measure of metabolism (von Caemmerer *et al*., 2014). Fractionation during CO_2 uptake and assimilation processes are thought to be the major factors affecting leaf $\delta^{13}C$ (Farquhar *et al.*, 1989). Post-photosynthetic fractionation, which includes all of the isotopic fractionation after Rubisco carboxylation, may also affect carbon isotope composition but its contribution to leaf $\delta^{13}C$ is not known (Brüggemann et al., 2011).

The relationship between *TE* and leaf $\delta^{13}C$ in C_3 plants has made it a useful trait when breeding C_3 crops (Farquhar *et al.*, 1984; Teulat *et al*., 2002; Rebetzke *et al*., 2002; Condon *et al*., 2004; Saranga *et al*., 2004). In C_3 plants, $\delta^{13}C$ is negatively correlated with the ratio of leaf intercellular to ambient CO_2 concentrations (C_i/C_a), which is driven mainly by the movement of CO_2 through stomata and the rate of CO_2 drawdown by Rubisco. As stomata close, transpiration is reduced and C_i/C_a decreases. Given the theoretical relationship between C_i/C_a and *TE* in C_3 plants, there is a positive correlation between *TE* and $\delta^{13}C$ (Faquhar *et al*., 1989; von Caemmerer *et al*., 2014).

The relationship between leaf $\delta^{13}C$ and *TE* in C_4 plants is more complex. Differences in isotopic fractionation between the photosynthetic types is clearly observed in the leaf $\delta^{13}C$ signatures. C_3 plants range in leaf $\delta^{13}C$ from -23 to -32 ‰, whereas C_4 plants range from -11 to -15 ‰ (O'Leary, 1988). The $\delta^{13}C$ of C_4 plants is not only related to C_i/C_a but also to the proportion of CO_2 fixed by phosphoenolpyruvate carboxylase that leaks out of the bundle sheath cells (leakiness: Φ) (Farquhar, 1983). In contrast to C_3 plants, the relationship between $\delta^{13}C$ and C_i/C_a in C_4 plants is positive except when $\Phi > 0.37$ (Cernusak *et al.* 2013). Although Φ has been shown to be < 0.3 and stable across many environmental conditions (Henderson *et al.*, 1992), the contribution of Φ variation to observed variation in leaf $\delta^{13}C$ is not completely understood. Even when Φ is constant, the variation in leaf $\delta^{13}C$ in response to changes in C_i/C_a is much smaller in C_4 compared to C_3 plants (Cernusak *et al.* 2013; von Caemmerer *et al*., 2014). These factors have limited the use of leaf $\delta^{13}C$ in C_4 plants. Additional studies that investigate variations in leaf $\delta^{13}C$ and identify the underlying mechanisms that control these differences will facilitate the use of leaf $\delta^{13}C$ as a proxy trait for *TE*.

Zea mays serves as an excellent biological system for studying photosynthesis and water use of C_4 plants because of its economic importance as a major crop (nearly 37 million hectares planted in United States in 2017, USDA-NASS), and because of the genetic resources available. In addition, there is tremendous genomic and phenotypic diversity between lines of *Z. mays*, which is greater at the DNA sequence level than between humans and chimpanzees (Tian *et al.*, 2009). These attributes have enabled *Z. mays* to be a model system for studying a variety of complex traits through the development of populations that represent the vast intraspecies diversity (Hansey *et al.*, 2011; Romay *et al.*, 2013; Wallace *et al.*, 2014; Zhang *et al.*, 2015). Recently in a greenhouse experiment Kolbe *et al*., (2017) assayed leaf $\delta^{13}C$ of the Nested Association Mapping

(NAM) founder lines, which were previously chosen to represent the genetic diversity across all maize inbreds (Flint-Garcia *et al.*, 2005; McMullen *et al*., 2009) and found substantial intraspecies variation. In this study, we focus on field-grown plants to identify factors that influence leaf $\delta^{13}C$ in *Z. mays*.

These results not only guide subsequent studies on leaf $\delta^{13}C$, but also provides evidence for the relationship between $\delta^{13}C$ and transpiration in a C_4 species.

RESULTS

Diversity of Leaf $\delta^{13}C$ in Field-Grown *Zea mays*

To assess the natural diversity of leaf $\delta^{13}C$ in field grown *Z. mays*, a set of 31 inbred lines were grown for two seasons at the University of Illinois (Table A.1). This set of lines included the 26 NAM founder lines, three inbreds commonly used in genetic studies and for transformation (Mo17, W22, and H99), as well as two Expired Plant Variety Protection (ExPVP) lines (LH82 and PH207). In 2015, the average leaf $\delta^{13}C$ across all lines was -12.14 ‰, with a range from -11.61 to -13.02 ‰. Slightly shifted, but similar trait values were observed in 2016, with an average leaf $\delta^{13}C$ of -12.67 ‰, with a range from -12.22 to -13.29 ‰. Although there are some genotypes that depart from a linear regression of the two years of data (Figure 2.1), a Pearson correlation showed a significant relationship ($r = 0.6987$; p-value < 0.0001). To further investigate the repeatability and genetic influence on leaf $\delta^{13}C$, we incorporated data from a previous study that measured leaf $\delta^{13}C$ on the NAM founder lines in a greenhouse experiment (Kolbe *et al.*, 2017). From these three different environments, we calculated broad sense heritability on a line mean basis and found leaf $\delta^{13}C$ to have a moderate heritability ($H^2 = 0.57$).

Leaf $\delta^{13}C$ Circadian Time-course

Although $\delta^{13}C$ is generally considered an integrated measure of carbon fixation, the potential effect of diurnal pools of photosynthate have not previously been evaluated. To determine if leaf $\delta^{13}C$ values change during a 24-hour period, we sampled the *Z. mays* reference line B73 at one-hour intervals in a circadian time-course experiment. An ANOVA was used to compare the individuals sampled across the 24-hour period and a significant difference was found between sampling times ($p = 0.0219$). A Tukey's *post hoc* pairwise comparison revealed that this

difference was due to a single time point (12:00) that was significantly lower than 5:00, 6:00, and 18:00. However, the differences do not resemble a pattern consistent with a diurnal mechanism. This result supports the use of leaf $\delta^{13}C$ as an integrated measurement of carbon fixation in the leaves and not a measure of active photosynthate, which would fluctuate diurnally. The pooled samples had an average leaf $\delta^{13}C$ value of -12.91 ‰ for the duration of the time-course. The maximum deviation of the pooled samples from their average was 0.24 ‰. This deviation is near expectation for technical measurement error. Samples collected and analyzed as individuals from each time point resulted in leaf $\delta^{13}C$ values consistent with pooled samples (Figure 2.2).

Leaf $\delta^{13}C$ Across *Zea mays* Development

To determine if leaf $\delta^{13}C$ values change during plant growth, the *Z. mays* reference line B73 was sampled as new leaves expanded throughout development over two growing seasons. These experiments showed variation in leaf $\delta^{13}C$ values across developmental time. In both years a trend emerged where leaves had less negative $\delta^{13}C$ values as they transitioned between juvenile and adult leaf stages. A mixed linear model was used to combine the data from the two years so that the trend could be further examined using Least Squared Means (Figure 2.3A). Leaves from juvenile growth stages (V4-V5) resulted in a lower average $\delta^{13}C$ value (-12.91 ‰) than adult leaves (V10-V19), which averaged -12.24 ‰. The data from both years places the transition in leaf $\delta^{13}C$ values near V7 in B73. After this transition, leaf $\delta^{13}C$ values stay relatively constant throughout mature growth including the flag leaf. From these results, we conclude that V10 is an optimal stage to sample leaf $\delta^{13}C$.

To assess whether differences in leaf $\delta^{13}C$ between juvenile and adult leaves was significant and common across lines of *Z. mays*, the 31 inbred lines previously grown to assess diversity were sampled at leaf stages V5 and V10. The juvenile $\delta^{13}C$ leaf samples were taken at V5 to reduce the possibility of sampling leaves that are composed primarily of carbon from the kernel, which can contribute significantly to the first few leaves. Sampling later than V5 would have introduced the possibility of inadvertently measuring within the stages of transition (V6-V8). A highly significant difference in $\delta^{13}C$ was observed between juvenile and adult leaves ($p < 0.0001$). The shift to less negative leaf $\delta^{13}C$ values (average V5 = -13.56 ‰ and V10 = -12.67 ‰) were consistent with what was observed with B73 (Figure 2.3B). Although all 31 lines

shifted in the same direction, the amount varied from 0.50 ‰ to 1.30 ‰ depending on the line, with an average of 0.79 ‰ across all lines (Figure A.1). Significant differences in leaf percent carbon ($p < 0.0001$), percent nitrogen ($p = 0.0090$), and $\delta^{15}N$ ($p = 0.0009$) were also observed between juvenile and adult leaves (Figure A.2).

To further investigate the difference in $\delta^{13}C$ observed between juvenile to adult leaves, samples were taken from wild-type and *glossy15* (*gl15*) mutants in two different *Z. mays* backgrounds (B73 and W64A). It is well known that *gl15* mutants have a reduced expression of juvenile leaf traits and show adult leaf characteristics at V3 (Moose and Sisco, 1994). Premature adult leaf traits include adult epidermal wax, adult cell wall characteristics, presences of epidermal hairs, and the presence of bulliform cells. Although only two replicates were grown for each genotype and were sampled as pools, no differences were observed between wild-type and *gl15* mutants in either background. At V5 the difference between wild-type and *gl15* mutant plants was -0.07 ‰ and 0.02 ‰ in B73 (average -13.03 ‰) and W64A (average -13.28 ‰) respectively. At V10 the difference between wild-type and *gl15* mutant plants was -0.06 ‰ and -0.16 ‰ in B73 (average -12.87 ‰) and W64A (average -12.83 ‰) respectively. Because no obvious differences were observed between wild-type and *gl15* mutants, these experiments were not repeated. These results suggest that epidermal leaf characteristics under the control of *Gl15* are not responsible for the differences in leaf $\delta^{13}C$ observed in juvenile and adult leaves.

Relationship Between Leaf $\delta^{13}C$ and Water Stress in *Zea mays*

A subset of lines with consistently extreme leaf $\delta^{13}C$ values were grown for three field seasons. This subset was made up of four Recombinant Inbred Lines (RILs) with high (less negative) leaf $\delta^{13}C$ values and four RILs with low (more negative) leaf $\delta^{13}C$ values. The high and low leaf $\delta^{13}C$ RIL groups had distinct isotopic signatures when grown in 2015 and 2016 (Figure 2.4; $p < 0.0001$). Both the 2015 and 2016 growing season had ample rainfall from the time of planting until the time of sampling (23.5 cm and 25.8 cm, respectively). The consistent difference between the high and low RIL groups is not present in 2017 (Figure 2.4), when there was no significant difference between the high and low RIL groups ($p = 0.0744$). Interestingly, 2017 was a dry year with only 14.0 cm of precipitation between planting and sampling, and plants showed drought phenotypes for much of the growing season.

Because the results of the field experiments suggested a link between leaf $\delta^{13}C$ and drought stress in *Z. mays*, a greenhouse experiment was performed to more precisely tease apart this relationship. Of the eight RILs grown in the field that had extreme isotope values, four were selected that had similar plant height and flowering time. The subset of RILs selected for the greenhouse experiment was comprised of two RILs with high leaf $\delta^{13}C$ values (Z007E0067 and Z021E0032) and two RILs with low leaf $\delta^{13}C$ values (Z007E0150 and Z021E0097), when measured in the field. To ascertain the effect of water availability on leaf $\delta^{13}C$, the four RILs were grown under three different water treatments: 100% field capacity (FC), 80% FC, and 40% FC.

A significant treatment effect was observed between 40% FC and both 100% and 80% FC with respect to the total amount of water transpired (p <0.00001; Figure 2.5). However, no difference in total transpiration was observed between the 100% and 80% FC treatments (p = 0.3547). A genotypic effect was observed with Z007E0067 transpiring significantly more than Z007E0150 at both 100% and 80% FC (p = 0.02527 and p = 0.0306 respectively; Figure 2.5, Figure A.3). No significant genotypic difference was observed for total transpiration when plants were grown at 40% FC (p =0.2260). However, all four RILs grown at 40% FC had significantly lower leaf $\delta^{13}C$ values (p <0.0001) than both the 100% and 80% FC treatments (Figure 2.5). A clear decrease in leaf $\delta^{13}C$ is observed as total transpiration is reduced (Figure 2.5). A genotypic effect was also seen in regards to leaf $\delta^{13}C$. Z007E0067 had significantly higher leaf $\delta^{13}C$ values than all other genotypes at 100% and 80% FC (p = 0.00044 and p = 0.00118 respectively; Table 2.1). For the 40% FC treatment, Z007E0150 and Z007E0067 had significantly higher $\delta^{13}C$ values when compared to Z021E0097 (p = 0.00114 and p = 0.03994 respectively; Table 2.1).

To investigate potential leaf level gas exchange differences between RILs, we collected steady state gas exchange measurements on all four RILs grown in the 100% FC treatment along with samples for leaf $\delta^{13}C$ at 54 days after planting (DAP). Line Z007E0150 had significantly lower values of net photosynthesis (A), stomatal conductance (g_s), and transpiration (E) compared to the other RILs (p <0.05; Table 2.2).In addition, Z007E0150 had the lowest C_i/C_a value (98.7 ± 4.6), which was significantly lower than Z007E0067 (130.8 ± 5.1; p = 0.0021). Z021E0032 also had a C_i/C_a significantly lower than Z007E0067 (p = 0.0266; Table 2.2). A comparison of leaf $\delta^{13}C$ collected at 54 DAP (corresponding to the gas exchange measurements) and at 64 DAP

(corresponding to the termination of the experiment) showed no significant differences in any of the four RILs (Figure A.4). Consistent with field measurements, Z007E0067 had a significantly higher leaf $\delta^{13}C$ ($p = 0.0004$); however, in the greenhouse Z021E0032 was statistically similar to the low leaf $\delta^{13}C$ RILs.

From this experiment both TE_{leaf} and TE_a were calculated at 100% FC. Leaf level transpiration efficiency, calculated using gas exchange measurements, showed that Z007E0150 had a significantly higher TE_{leaf} compared to Z007E0067 and Z021E0097 ($p = 0.0006$, $p = 0.0237$; Table 2.2). Agronomic transpiration efficiency, calculated using biomass and total water transpired, also showed that RIL Z007E0150 had a significantly higher TE_a than Z007E0067 and Z021E0097 ($p = 0.0006$ and $p = 0.0059$ respectively; Table 2.3). Z021E0032 had significantly higher *TE* than Z007E0067, but only when calculating TE_a ($p = 0.0262$). To further investigate what was driving TE_a differences between RIL lines, we looked closer at plant biomass. No significant difference in biomass was found between RILs at 100% FC ($p = 0.43$), indicating that the difference in TE_a are mainly attributable to total transpiration. However, significant differences were observed in plant height and leaf number (Table 2.3). Most notably, Z007E0150 is one of the taller RILs but has significantly fewer leaves, whereas Z007E0067 is the shortest RIL and has the most leaves (Table 2.3).

To determine the correlation between traits measured during the greenhouse experiment, a correlation matrix was generated using traits collected in all three water treatments (Figure 2.6). As expected, strong negative correlations were found between total transpiration and TE_a as well as between biomass and TE_a because both total transpiration and biomass are used to calculate TE_a. However, a negative correlation was also observed between TE_a and $\delta^{13}C$ values. Large positive correlations were found between leaf $\delta^{13}C$ values and total transpiration, leaf $\delta^{13}C$ values and biomass, and total transpiration and biomass.

DISCUSSION

Despite the complexity of isotopic fractionation in C_4 species, the use of leaf $\delta^{13}C$ has been proposed as a method for measuring *TE* in *Z. mays*. Here we specifically test field-grown *Z. mays* and sources of variation in sampling leaf $\delta^{13}C$. These results facilitate the standardization

and selection of the appropriate sampling time to maximize the effectiveness of leaf $\delta^{13}C$ measurements. Furthermore, we specifically test the relationship between *TE* and leaf $\delta^{13}C$ in the greenhouse. These results open up specific targets for the optimizing of water-use efficiency in a major C_4 crop.

The 31 inbred lines of *Z. mays* sampled in this study had a trait distribution for leaf $\delta^{13}C$ that spans a large portion of the range seen across all C_4 species (-11 to -15 ‰; O'Leary, 1988). Because the observed variation has a moderate genetic heritability, this trait has the potential to be used in a breeding program. The heritability for leaf $\delta^{13}C$ is similar to what has previously been reported in *Z. mays* (0.51; Foley, 2012). Because our goal was to assess natural genetic variation in leaf $\delta^{13}C$, the lines sampled were selected to maximize diversity. Therefore, only two ExPVP lines were included in this study. Thus, it is not possible with this data set to assess the amount of variability for leaf $\delta^{13}C$ found in temperate elite germplasm compared to the diverse NAM founder lines. However, both of the ExPVP lines were found to have values at the high (less negative) end of the trait distribution, possibly indicating that there are alleles from diverse material that could lower leaf $\delta^{13}C$ values.

Similar variation in leaf $\delta^{13}C$ was reported for the NAM Founder lines when grown in the greenhouse (Kolbe *et al.*, 2017). Although many of the lines were stable in their relative position in the distribution, the absolute value of the trait distribution seen in the greenhouse was shifted to more negative leaf $\delta^{13}C$ values. While there are many differences between greenhouse and field-grown plants, this shift is likely due to the differences in the atmospheric concentration of ^{13}C between greenhouse (-11 ‰; Kolbe *et al.*, 2017) and field (typically -8 ‰) environments. The shift to more negative leaf $\delta^{13}C$ values is also visible in our greenhouse experiment when compared to field-grown plants of the same RILs. While most of the lines were relatively consistent between greenhouse and field environments, some lines had significant genotype by environment interactions as seen by the drastic change of their relative rank. In particular, CML247 and W22 had high leaf $\delta^{13}C$ values in the greenhouse but consistently low leaf $\delta^{13}C$ in the field. The opposite was true for CML228. A genotype by environment interaction was also observed with RIL Z021E0032. This would suggest that greenhouse screens of leaf $\delta^{13}C$ are useful, but would need to be supported with field experiments to confirm the phenotype.

The investigation of variation in sampling with respect to circadian and developmental time revealed periods of stable leaf $\delta^{13}C$. Here we performed a formal testing of the hypothesis that leaf $\delta^{13}C$ is an integrated measurement of fixed carbon rather than an instantaneous measure of the active photosynthetic pool. The relative stability of leaf $\delta^{13}C$ over the circadian time-course experiment indicates the time at which the sample is taken during the day has no effect on the isotopic signature. Unlike the stability seen over a 24-hour period, there was a significant trend in leaf $\delta^{13}C$ over developmental time. Over multiple years and across a diverse panel of lines, there was a significant difference between leaf $\delta^{13}C$ in juvenile and adult leaves. The timing of transition from low to high leaf $\delta^{13}C$ seen in this study is similar to what was measured previously in a coarse developmental time series (Zhang *et al.*, 2015). Although the difference in leaf $\delta^{13}C$ through development was not as large as between genotypes, an average difference of 0.79 ‰ was observed between V5 and V10 leaves (Figure 2.2B).

At this point, it is not clear what process is driving the difference in leaf $\delta^{13}C$ between juvenile and adult leaves. Interestingly, the timing of the change is similar to vegetative phase change timing in *Z. mays*. An obvious indicator of this transition is the change from juvenile to adult epicuticular wax, which occurs around V7 in B73 (Foerster *et al*, 2015). Due to the possible connection, differences in vegetative phase change timing between lines should be considered when sampling. However, >95% of the 4,018 NAM RILs tested transitioned before V10 (Foerster *et al*, 2015), which supports our conclusion that V10 is near optimal for sampling leaf $\delta^{13}C$. Although later leaf stages are stable with respect to leaf $\delta^{13}C$, other differences between lines are compounded as the growing season progresses. Our analysis of *gl15* mutants suggests that the difference in leaf $\delta^{13}C$ is not due to changes in epicuticular wax. In addition to changes in epicuticular wax, several other leaf characteristics change during the juvenile to adult phase change including thickening of the cuticle, changes in epidermal cell walls, presences of epidermal hairs, and the presence of bulliform cells (Poethig, 1990; Moose and Sisco, 1994). The effect of cuticle thickness on leaf $\delta^{13}C$ is still not known because it is not controlled by *Gl15* (Evans *et al.*, 1994). In addition to leaf morphology, it is also possible that the difference in leaf $\delta^{13}C$ is due to physiological differences between juvenile and adult leaves. This could include differences in stomatal opening that could cause a low C_i/C_a in juvenile leaves. Alternatively, the difference in leaf $\delta^{13}C$ may not be due to characteristics of the juvenile leaf per se, but rather it

could be due to the carbon signature from the previous generation, which contributes significantly to juvenile leaves through seed reserves.

Previous reports on the effect of drought on leaf $\delta^{13}C$ in *Z. mays* have been inconsistent (Monneveux et al., 2007; Zhang *et al.*, 2015). Theoretically, different trends are possible if Φ significantly changes under drought stress. When Φ is > 0.37, a negative relationship between $\delta^{13}C$ and C_i/C_a is predicted; however, if Φ is < 0.37, a positive relationship between $\delta^{13}C$ and C_i/C_a is predicted (Cernusak *et al.* 2013). Although estimates of Φ from gas exchange measurements and dry leaf $\delta^{13}C$ have documented substantial changes in Φ in response to environmental differences, the more accurate measure of Φ calculated from instantaneous measurements of carbon isotope discrimination is relatively constant under different irradiances, temperatures, and CO_2 concentrations (Kromdijk *et al.*, 2014). However, because there is a lack of direct measurements of Φ under water limiting conditions, the extent to which Φ influences leaf $\delta^{13}C$ under these conditions is not known. Our data show a clear decrease in leaf $\delta^{13}C$ under water limiting conditions for field-grown plants as well as plants grown under controlled water stress experiments in the greenhouse. This result is consistent with a Φ < 0.37 where the reduction in C_i/C_a in response to water limitations is the major driver of leaf $\delta^{13}C$ under drought. A similar result was found in the C_4 grasses *Setaria viridis* and *Setaria italica* (Ellsworth *et al.*, 2017). However, our data from the greenhouse experiment indicates that while C_i/C_a may be a major factor, it is not the only thing effecting leaf $\delta^{13}C$, as seen by directly comparing C_i/C_a to leaf $\delta^{13}C$ (Table 2.1 and 2.2). Other factors such as mesophyll conductance could also be contributing to leaf $\delta^{13}C$, but it is predicted that the effect of mesophyll conductance on leaf $\delta^{13}C$ in C_4 plants is small (von Caemmerer *et al*., 2014).

The response of leaf $\delta^{13}C$ to water limitation in the field, and the greenhouse, has several implications for leaf $\delta^{13}C$ use as a proxy trait for water-use efficiency. Under severe drought it is possible that C_i/C_a approaches a biological limit that drives leaf $\delta^{13}C$ values to be more negative and nearly uniform across all lines. If there is a lower limit to C_i/C_a, it is interesting to speculate that the small differences observed in leaf $\delta^{13}C$ between lines grown under drought conditions may reflect the amount of variation in other processes (such as Φ or post photosynthetic fractionation) that contribute to leaf $\delta^{13}C$. Regardless, these results seem to suggest that measurements of leaf $\delta^{13}C$ may only be informative in assessing *TE* under well-watered

conditions. Under 100% FC in the greenhouse, Z007E0067 had the highest transpiration and also had a significantly higher leaf $\delta^{13}C$ compared to the other RILs. Thus, selection for leaf $\delta^{13}C$ under well-watered conditions may provide a breeding target for improving *TE* and the sustainability of *Z. mays* production under current and future growing environments.

MATERIALS AND METHODS

Plant Growth

All field trials were grown at the Crop Sciences Research and Education Center located in Urbana, Illinois. Fifteen kernels were planted in each 3.7 meter row with 0.8 meter spacing between rows and 0.9 meter alleys. The fields were planted on May 14th 2015, May 7th 2016, and May 16th 2017. No irrigation was provided for any of the experiments. All 31 *Z. mays* inbred lines used in these experiments are publicly available through the USDA Germplasm Resources Information Network (GRIN). These inbreds were planted as a single block arranged according to flowering time in 2015 and 2016. The *glossy15-H* allele used in this study was previously described by Moose and Sisco (1996), and were planted in two single row plots in 2016. Plants were sampled at the developmental stage indicated for each experiment.

The RIL greenhouse experiment was conducted at the University of Illinois Plant Care Facility located in Urbana, Illinois. NAM RILs used in this experiment are available from the Maize Genetics Stock Center. Kernels were sown in 50 cell trays filled with LC1 soilless media (SunGro Sunshine Mix #1). Plants were grown in the greenhouse under supplemental metal halide lighting set to 14 hour days. Prior to transplanting into Classic® 2000 pots, a coffee filter was placed at the bottom of each pot to prevent any media from being lost and each pot was filled with the same volume of media. The media used was 3:1:1:1 of LC1, sterilized field soil, peat, and perlite respectively. The field capacity of the pots was determined by saturating the soil for 3 days and weighing each pot once the excess water had run through the media. The pots were then dried in a drier with continuous airflow at 60°C. Pots were periodically weighed until their weight remained constant thus signifying complete dry down, which occurred after 15 days. The difference for each pot between saturated soil and dry down was determined to be the weight of available water. This difference was averaged to determine the amount of water at field

capacity (FC). The weight of 80% and 40% FC was calculated for each water treatment. Seedlings were transplanted into pots 17 days after planting (DAP) and the pots were arranged in a randomized complete block design. Soil amendments for fertility were added to the pots during transplanting which included: Osmocote® (11-4-17), dolomitic lime, phosphorous, magnesium sulfate, and gypsum. Plants were well watered until the start of the experiment. The fungicide Pagent® was applied directly after transplanting. For the duration of the experiment the pots were fertilized with 500 mL of 300 ppm (15-5-15) CalMag every 7 days. Before the water treatments began, each pot was weighed with the 21 day seedling and the treatment weight was calculated. The water treatment began 33 DAP. Each morning at the beginning of the light period, the pots were weighed and the difference between the previous day's weight was calculated and the weight lost through evapotranspiration was replaced with the equivalent weight of water. In each water treatment replication there was a pot without a plant which served as an evaporation control. This allowed daily transpiration of each plant to be measured over the course of the treatment period (Figure A.3). The experiment was terminated 64 DAP and leaf samples were taken from the upper most fully expanded leaf for isotopic analysis. Aboveground biomass was taken by cutting the plant at the soil surface and drying it at 60°C for 14 days. Total water use was calculated by summing the difference in weight each day and subtracting the difference in weight of the evaporation control pot per each treatment. TE_a was calculated by the aboveground biomass (g) over the total volume of water used during the treatment (L).

Gas exchange measurements were taken on the uppermost fully expanded leaf using a LICOR-6800 over three days starting 50 DAP. The uppermost fully expanded leaf was leaf 9 (V9) in all measured plants. Only plants from the 100% FC treatment group were measured. Five plants from each line were measured; with the exception of Z021E0097, only four plants were measured due to the loss of one replicate. All leaf chamber conditions were set constant during measurements. The temperature of the exchanger was set at 25^{o}C and H_2O concentrations were controlled automatically to maintain a constant VPD of 1.5 kPa. The CO_2 concentration of the chamber was set constant at 400 μmol mol^{-1} for the duration of measurements and light was set at 1,500 μmol m^{-2} s^{-1}. Each plant was acclimated to the chamber conditions for 15-30 minutes until steady state was achieved. Once the leaf reached steady-state, data was logged every 60 seconds for a duration of 5 minutes. Average net photosynthesis (A), stomatal conductance (g_s), and transpiration (E) were calculated for each line and an ANOVA and Tukey's *post hoc* tests

were ran to determine significant differences. Leaf level transpiration efficiency was calculated using the equation (*A*/*E*) and an ANOVA with Tukey's *post hoc* test was run to determine significant difference between lines. Leaf samples for isotopic analysis were taken from the portion of the leaf that was measured via the Licor 54 DAP.

Leaf Sample Collection

All samples for isotope analysis were collected from the middle of the leaf blade (avoiding the midrib) of the uppermost fully expanded leaf using a 0.5 cm diameter single hole punch (Office Depot #825232). Only healthy leaf tissue was sampled to avoid confounding factors. Leaf samples were collected from individual plants or as pools of multiple plants from a single row depending on the experiment. Individual samples consisted of 12-24 punches total, half taken from each side of the midrib from the same leaf of a single plant. Pooled samples consisted of 6 punches from four individual plants from a single row. Leaf punches were placed in 2 mL Simport tubes with screw caps (VWR # 89499-598). Three 1/8" Grade 1000 Type 430 Stainless Steel ball bearings (Abbott Ball Company) were added to each tube for grinding. After collection, tubes containing tissue samples were uncapped and placed in a dryer at 65^{o}C for at least 7 days. Tubes were then capped and placed in a Nalgene desiccation cabinet (VWR # 24987-056) containing Drierite until the samples were prepared for isotope analysis. For the circadian time-course experiment, samples were taken from three randomly selected individuals at each time point from a large block of B73 plants. Plants were only sampled once during the experiment, and thus the data represents 72 individual plants. The δ^{13}C of three plants were measured individually and also as a combined pool.

Stable Carbon Isotope Analysis

Dry leaf tissue was ground in the Simport tubes with ball bearings by shaking in a Geno Grinder at 1000 rpm for 10 minutes. Ground leaf tissue was weighed out into 6 mm x 4 mm tin capsules (OEA Laboratories # C11350.500P) using a Sartorius CPA2P scale. The range of acceptable sample weight varied between isotope facilities. Samples were placed in a Costar 96-well plate and stored in the desiccation cabinet until it was analyzed. Samples were run through a Costech instruments elemental combustion system and then either a Delta V Advantage (University of

Illinois) or a Delta PlusXP (Washington State University) isotope ratio mass spectrometer to determine $\delta^{13}C$ values. The precision of the instruments measuring $\delta^{13}C$ is 0.2 ‰. Samples for the Diversity (2015), Circadian time-course (2016), B73 Development (2015), and greenhouse experiments were analyzed at The University of Illinois Urbana-Champaign. Samples for the Diversity (2016), B73 Development (2016), Juvenile/Adult leaves (2016), *gl15* experiment, and RILs (2015, 2016, 2017) were analyzed at Washington State University. The use of Vienna Peedee Belemnite calibrated standards permits the direct comparison of leaf $\delta^{13}C$ from different facilities.

Statistical Analyses

All statistical tests and data visualizations were performed using statistical packages in R (R Development Core Team, 2010). Graphs were made using the *boxplot* function or using the package *ggplot2*. A linear model was used for the B73 Development experiment to combine the data from 2015 and 2016 using the package *lme4*. Least Squares means were then calculated using the package *lsmeans*. One way ANOVAs were used to test for significant differences between data points in the B73 Developmental experiment, the Circadian time-course, and greenhouse experiment. Tukeys HSD with an alpha of 0.05 was performed using the package *multcomp* after each significant ANOVA test. A Pearson correlation test was performed to calculate the linear dependence of the response variables to each other. The correlation matrix was constructed using the package *corrplot*. Heritability of leaf $\delta^{13}C$ was calculated using NAM Founder data from 2015 and 2016 described in this study. Data from Kolbe *et. al.*, (2017) was also used in the heritability calculation, which included three replicates of each of the NAM founder lines and six replicates of the reference line B73 grown in the greenhouse. Therefore, the calculation included three environments and 27 genotypes. First the variance components were estimated using *lme4*. Then broad sense heritability on a line mean basis was calculated using the equation

$$H^2 = \sigma_g^2 / (\sigma_g^2 + (\sigma_{ge}^2/m) + (\sigma^2/m)$$

where σ_g^2 is the genotypic variance, σ_{ge}^2 is the genotype:environement variance, σ^2 is the error variance, and m is the number of environments, as described previously Piepho and Möhring, 2007).

ACKNOWLEDGEMENTS

We thank Dr. Steve Moose for providing seed for the *glossy15* experiment. We would also like to thank Mengqiao Han for her technical help in isotope preparation and thoughtful discussion during manuscript preparation. This work was supported by United States Department of Agriculture through Hatch funds.

FIGURES AND TABLES

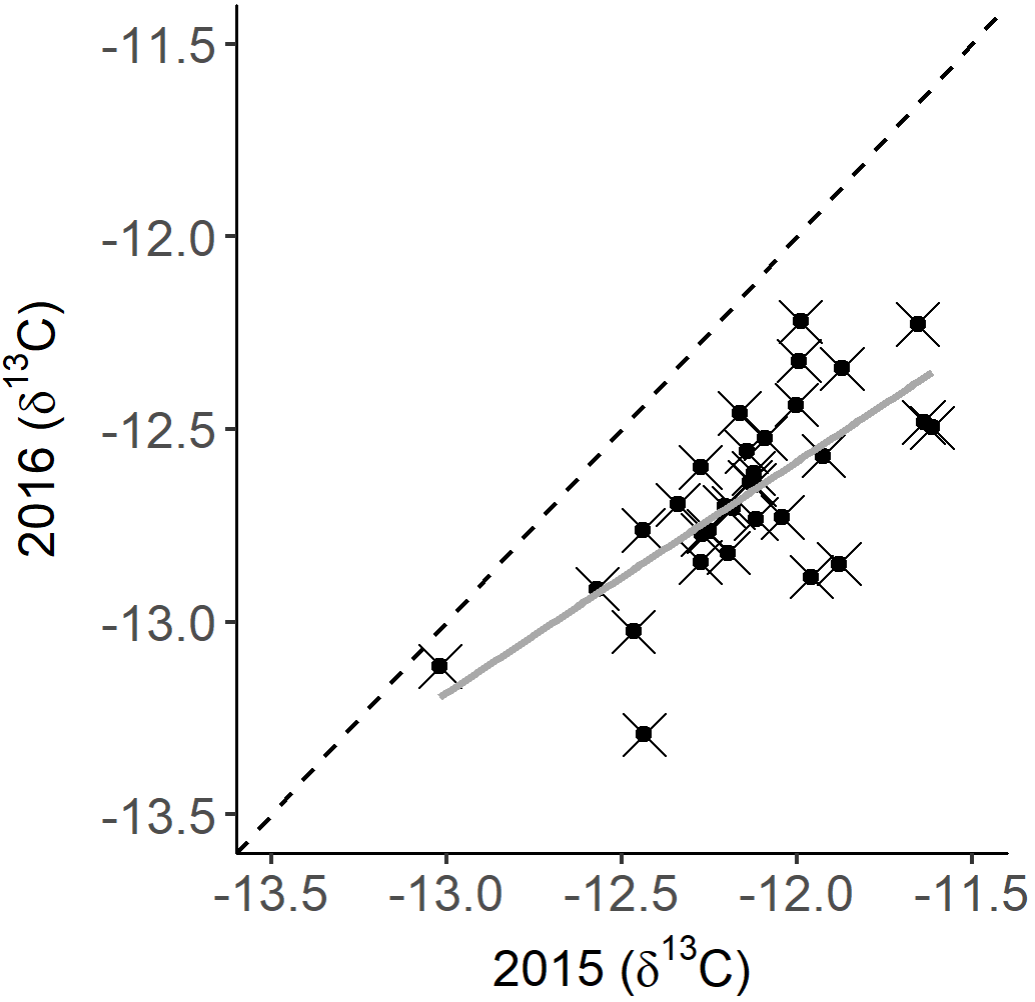

Figure 2.1: Comparison of leaf $\delta^{13}C$ values from two individual field seasons.

Data points represent leaf $\delta^{13}C$ values measured in two consecutive years during mature growth.

A linear best-fit line is shown in grey, and the dashed line shows a 1:1 relationship.

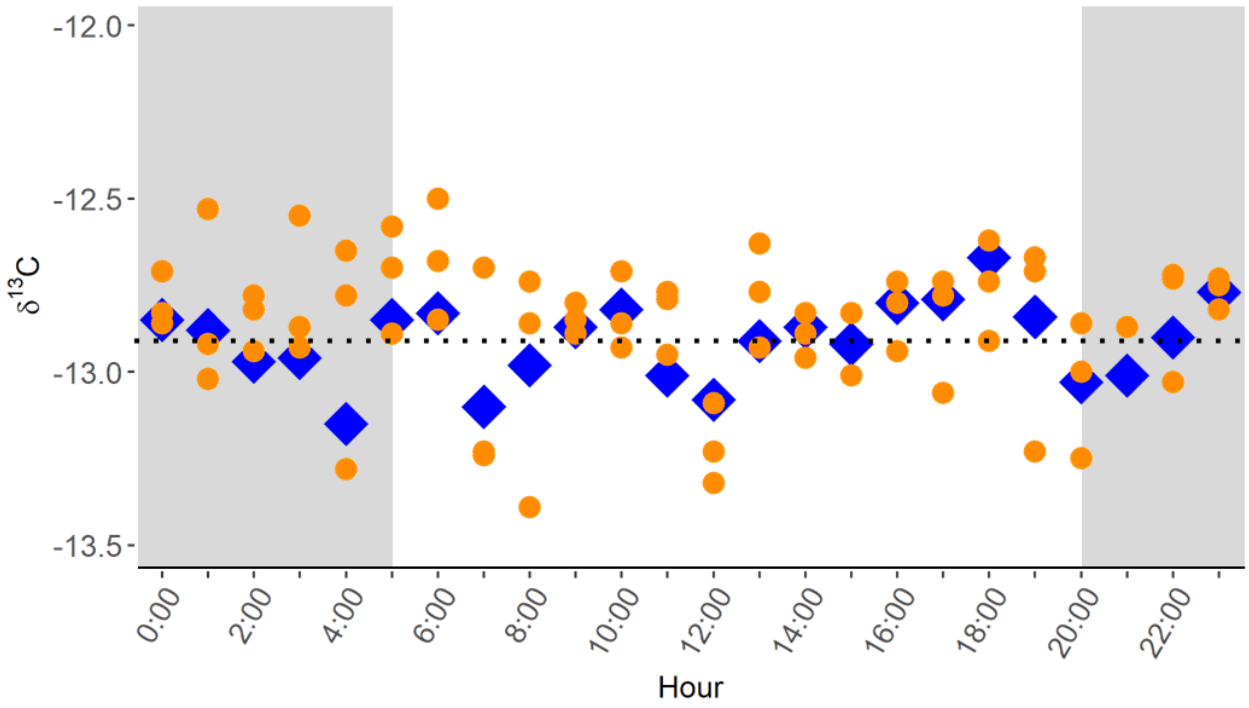

Figure 2.2: Circadian time-course of leaf $\delta^{13}C$ in *Z. mays*.

Data points represent leaf $\delta^{13}C$ values of a single *Z. mays* line (B73) collected hourly for a duration of 24 hours. Blue diamonds show leaf $\delta^{13}C$ values of pooled samples and orange circles show leaf $\delta^{13}C$ values of individual plants that compose each pool. The horizontal dashed line represents the average leaf $\delta^{13}C$ value (-12.91 ‰) for all pooled samples during the 24 hour collection period. Shaded areas of the graph represent time of darkness between sunset and sunrise.

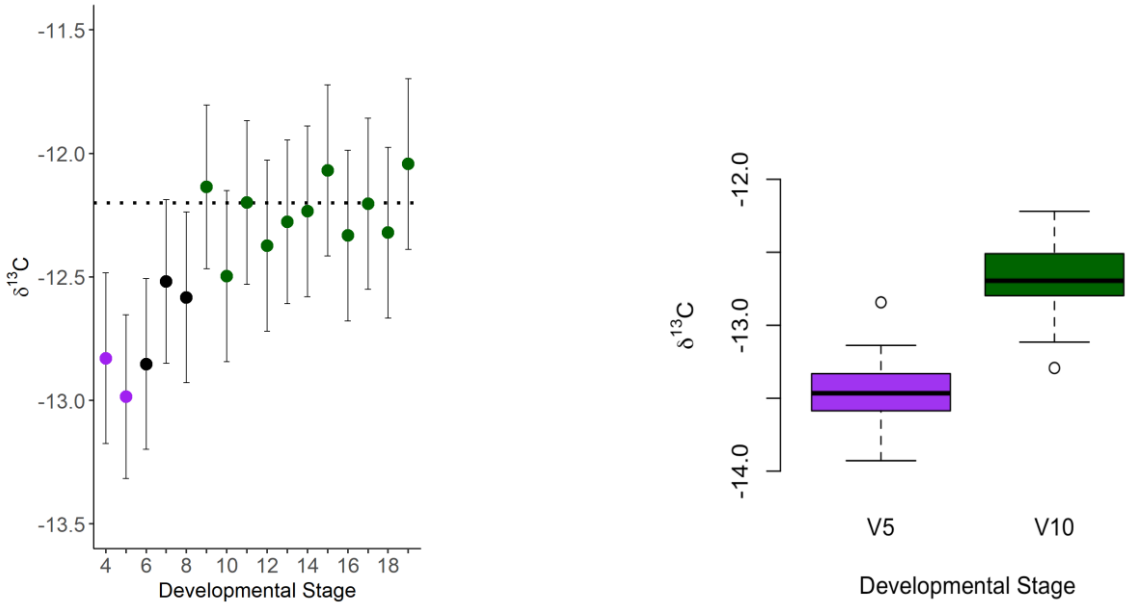

Figure 2.3: Developmental variation of leaf $\delta^{13}C$ in *Z. mays*.

(a) Data points represent Least Squares Mean of leaf $\delta^{13}C$ values calculated for each developmental stage over two independent field seasons. V-stage is shown on the x-axis. Error bars show standard error and horizontal dashed line represents the average leaf $\delta^{13}C$ value (-12.2 ‰) of mature leaf stages (V9-V19). Colors show the trend from juvenile (purple), thru transition (black), to adult (green). (b) The inset boxplots show juvenile and adult leaf $\delta^{13}C$ values for 31 *Z. mays* lines. The box shows the 1st and 3rd quartile with horizontal lines indicating the mean and the whiskers showing the mild outliers. Open circles represent the extreme outliers.

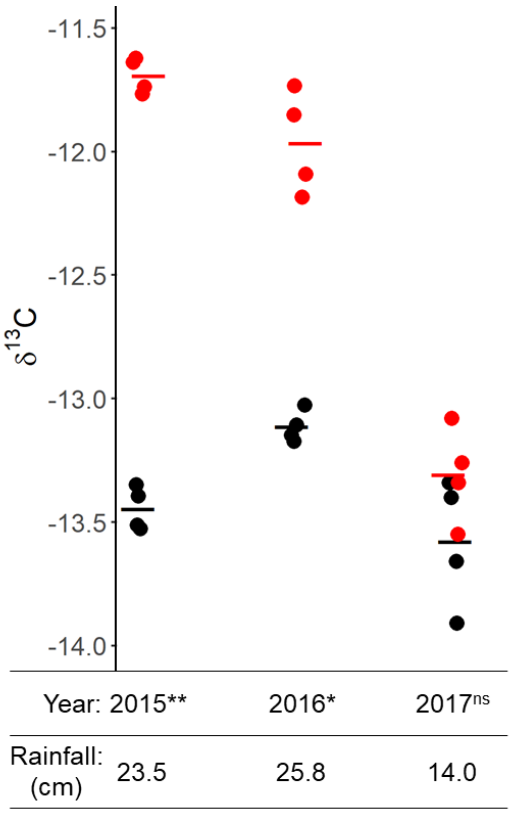

Figure 2.4: Response of leaf $\delta^{13}C$ to water limiting conditions.

Points represent leaf $\delta^{13}C$ values of eight RILs grown in three consecutive field seasons.

Horizontal lines indicate averages of the "high" (red) and "low" (black) RIL groups in each year.

Rainfall totals (in centimeters) from the time of planting to sampling are shown below each year.

** $p = 3.685 \times 10^{-8}$, * $p = 2.185 \times 10^{-5}$, ns (not significant).

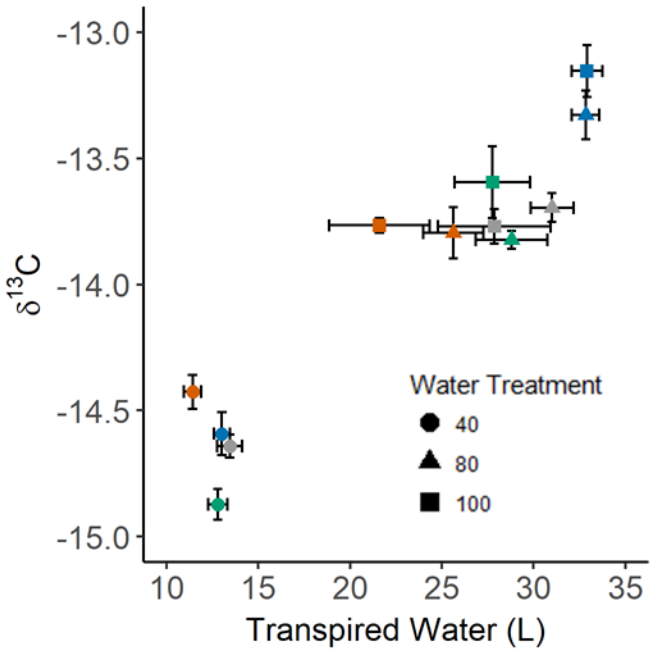

Figure 2.5: Leaf $\delta^{13}C$ compared to transpiration of four *Z. mays* RILs grown in the greenhouse under three water treatments.

Gray (Z021E0032), orange (Z007E0150), green (Z021E0097), and blue (Z007E0067) points represent means of the RILs grown in each treatment. Bars show standard error of the mean. Shape of the points distinguish 100%, 80%, and 40% FC treatment. The treatment effect between 100% FC and 80% FC was not significant, but the treatment effect between 40% FC and both 80% FC and 100% FC was significant at $p < 0.00001$.

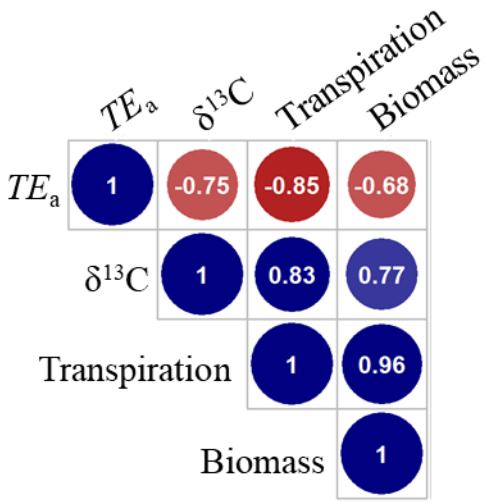

Figure 2.6: Pearson coefficient for phenotypic traits recorded for all water treatments. Blue shades represent positive correlations while red shades represent negative correlations. The size of the circles represent the strength of correlation with larger circles representing stronger correlations.

Table 2.1. Stable Carbon Isotope Values of Greenhouse Grown RILs.

Genotype	100% FC 54 DAP ($\delta^{13}C$)	100% FC 64 DAP ($\delta^{13}C$)	80% FC 64 DAP ($\delta^{13}C$)	40% FC 64 DAP ($\delta^{13}C$)
	‰	‰	‰	‰
Z007E0067	-13.18 ± 0.03 [a]	-13.15 ± 0.10 [a]	-13.33 ± 0.10 [a]	-14.59 ± 0.09 [a]
Z007E0150	-13.64 ± 0.05 [b]	-13.77 ± 0.03 [b]	-13.80 ± 0.10 [b]	-14.43 ± 0.07 [a]
Z021E0032	-13.60 ± 0.02 [b]	-13.77 ± 0.07 [b]	-13.70 ± 0.06 [b]	-14.64 ± 0.05 [ab]
Z021E0097	-13.70 ± 0.04 [b]	-13.60 ± 0.14 [b]	-13.82 ± 0.04 [b]	-14.87 ± 0.06 [b]

Presented as average ± standard error. Significance threshold of $p < 0.05$.

Table 2.2. Gas Exchange Measurements of 100% FC Greenhouse Grown RILs.

Genotype	Net Photosynthesis (A)	Stomatal conductance (g_s)	Transpiration (E)	Intercellular CO_2/ Atmospheric CO_2 (C_i/C_a)	TE_{leaf} (A/E)
	µmol m^{-2} s^{-1}	mol m^{-2} s^{-1}	mol m^{-2} s^{-1}	µmol mol^{-1}	µmol m^{-2} s^{-1} mol m^{-2} s^{-1}
Z007E0067	32.2 ± 0.7 [a]	0.268 ± 0.012 [a]	0.0039 ± 0.0002 [a]	0.3852 ± 0.0155 [a]	8406.86 ± 252.15 [b]
Z007E0150	27.2 ± 0.5 [b]	0.185 ± 0.004 [b]	0.0027 ± 0.0001 [b]	0.2825 ± 0.0130 [b]	10024.77 ± 177.28 [a]
Z021E0032	34.3 ± 1.0 [a]	0.260 ± 0.011 [a]	0.0038 ± 0.0002 [a]	0.3215 ± 0.0115 [b]	9151.14 ± 200.11 [ab]
Z021E0097	32.3 ± 1.7 [a]	0.250 ± 0.017 [a]	0.0036 ± 0.0002 [a]	0.3419 ± 0.0219 [ab]	8930.24 ± 292.95 [b]

Presented as average ± standard error. Significance threshold of $p < 0.05$.

Table 2.3. Agronomic Measurements of Greenhouse Grown RILs.

Genotype	100% FC Biomass	80% FC Biomass	40% FC Biomass	100% FC Height	100% FC Leaf Number	100% FC TE_a
	g	g	g	cm		g L^{-1}
Z007E0067	142.4 ± 5.9 [a]	148.0 ± 7.1 [ab]	77.6 ± 4.6 [a]	130.0 ± 5.7 [b]	20.2 ± 0.4 [a]	4.35 ± 0.12 [c]
Z007E0150	125.0 ± 12.7 [a]	139.0 ± 7.0 [ab]	73.0 ± 2.5 [a]	151.6 ± 3.5 [a]	17.4 ± 0.2 [c]	5.91 ± 0.35 [a]
Z021E0032	146.6 ± 13.0 [a]	163.4 ± 4.6 [a]	82.0 ± 1.7 [a]	137.0 ± 5.3 [ab]	18.8 ± 0.2 [b]	5.32 ± 0.14 [ab]
Z021E0097	128.3 ± 9.0 [a]	134.0 ± 5.9 [b]	76.4 ± 2.4 [a]	157.4 ± 4.2 [a]	20.0 ± 0.0 [a]	4.63 ± 0.16 [bc]

Presented as average ± standard error. Significance threshold of $p < 0.05$.

REFERENCES

Blum, A. (2009). Effective use of water (EUW) and not water-use efficiency (WUE) is the target of crop yield improvement under drought stress. *Field Crops Res.*, *112*, 119-123.

Brüggemann, N., Gessler, A., Kayler, Z., Keel, S.G., Badeck, F., Barthel, M., Boeckx, P., Buchmann, N., Brugnoli, E., Esperschütz, J., and Gavrichkova, O. (2011). Carbon allocation and carbon isotope fluxes in the plant soil-atmosphere continuum: a review. *Biogeosciences*, *8*, 3457-3489.

Cernusak, L.A., Ubierna, N., Winter, K., Holtum, J.A., Marshall, J.D., and Farquhar, G.D. (2013). Environmental and physiological determinants of carbon isotope discrimination in terrestrial plants. *New Phytol.*, *200*, 950-965.

Condon, A.G., Richards, R.A., Rebetzke, G.J., and Farquhar, G.D. (2004). Breeding for high water-use efficiency. *J. Exp. Bot.*, *55*, 2447-2460.

Dhanapal, A.P., Ray, J.D., Singh, S.K., Hoyos-Villegas, V., Smith, J.R., Purcell, L.C., King, C.A., Cregan, P.B., Song, Q., and Fritschi, F.B. (2015). Genome-wide association study (GWAS) of carbon isotope ratio (δ13C) in diverse soybean [Glycine max (L.) Merr.] genotypes. *Theor. Appl. Genet.*, *128*, 73-91.

Ellsworth, P.Z., and Cousins, A.B. (2016). Carbon isotopes and water use efficiency in C_4 plants. *Curr. Opin. Plant Biol.*, *31*, 155-161.

Ellsworth, P.Z., Ellsworth, P.V., and Cousins, A.B. (2017). Relationship of leaf oxygen and carbon isotopic composition with transpiration efficiency in the C_4 grasses *Setaria viridis* and *Setaria italica*. *J. Exp. Bot.*, *68*, 3513-3528.

Evans, M.M., Passas, H.J., znd Poethig, R.S. (1994). Heterochronic effects of *glossy15* mutations on epidermal cell identity in maize. *Genes Devel.*, *120*, 1971-1981.

Farquhar, G.D. (1983). On the nature of carbon isotope discrimination in C_4 species. *Funct. Plant Biol.*, *10*, 205-226.

Farquhar, G.D., and Richards, R.A. (1984). Isotopic composition of plant carbon correlates with water-use efficiency of wheat genotypes. *Funct. Plant Biol.*, *11*, 539-552.

Farquhar, G.D., Ehleringer, J.R., and Hubick, K.T. (1989). Carbon isotope discrimination and photosynthesis. *Ann. Rev. Plant Biol.*, *40*, 503-537.

Foerster, J.M., Beissinger, T., de Leon, N., and Kaeppler, S. (2015). Large effect QTL explain natural phenotypic variation for the developmental timing of vegetative phase change in maize (*Zea mays* L.). *Theor. Appl. Genet.*, *128*, 529-538.

Foley R.C. (2012). The genetic diversity of water use efficiency in the nested association mapping population of Zea mays. Masters thesis, Department of Horticulture and Landscape Architecture, Purdue University.

Flint-Garcia, S.A., Thuillet, A.C., Yu, J., Pressoir, G., Romero, S.M., Mitchell, S.E., Doebley, J., Kresovich, S., Goodman, M.M., and Buckler, E.S. (2005). Maize association population: a high-resolution platform for quantitative trait locus dissection. *Plant J.*, *44*, 1054-1064.

Hall, A.J., and Richards, R.A. (2013). Prognosis for genetic improvement of yield potential and water-limited yield of major grain crops. *Field Crops Res.*, *143*, 18-33.

Hansey, C.N., Johnson, J.M., Sekhon, R.S., Kaeppler, S.M., and Leon, N.D. (2011). Genetic diversity of a maize association population with restricted phenology. *Crop Sci.*, *51*, 704-715.

Henderson, S.A., Caemmerer, S.V., and Farquhar, G.D. (1992). Short-term measurements of carbon isotope discrimination in several C_4 species. *Funct. Plant Biol.*, *19*, 263-285.

Kim, T.H., Böhmer, M., Hu, H., Nishimura, N., and Schroeder, J.I. (2010). Guard cell signal transduction network: advances in understanding abscisic acid, CO_2, and Ca_2^+ signaling. *Ann. Rev. Plant Biol.*, *61*, 561-591.

Kolbe A.R., Studer A.J., Cousins A.B. (2017). Biochemical and transcriptomic analysis of maize diversity to elucidate drivers of leaf carbon isotope composition. *Funct. Plant Biol.*, FP17265.

Kromdijk, J., Ubierna, N., Cousins, A.B., and Griffiths, H. (2014). Bundle-sheath leakiness in C_4 photosynthesis: a careful balancing act between CO_2 concentration and assimilation. *J. Exp. Bot*, *65*, 3443-3457.

Lobell, D.B., Roberts, M.J., Schlenker, W., Braun, N., Little, B.B., Rejesus, R.M., and Hammer, G.L. (2014). Greater sensitivity to drought accompanies maize yield increase in the US Midwest. *Science*, *344*, 516-519.

Long, S.P., and Bernacchi, C.J. (2003). Gas exchange measurements, what can they tell us about the underlying limitations to photosynthesis? Procedures and sources of error. *J. Exp.Bot.*, *54*, 2393-2401.

McMullen, M.D., Kresovich, S., Villeda, H.S., Bradbury, P., Li, H., Sun, Q., Flint-Garcia S., Thornsberry J., Acharya C., Bottoms C., and Brown, P. (2009). Genetic properties of the maize nested association mapping population. *Science*, *325*, 737-740.

Monneveux, P., Sheshshayee, M.S., Akhter, J., and Ribaut, J.M. (2007). Using carbon isotope discrimination to select maize (*Zea mays* L.) inbred lines and hybrids for drought tolerance. *Plant Sci.*, *173*, 390-396.

Moose, S.P., and Sisco, P.H. (1994). *Glossy15* controls the epidermal juvenile-to-adult phase transition in maize. *Plant Cell*, *6*, 1343-1355.

Moose, S.P., and Sisco, P.H. (1996). *Glossy15*, an APETALA2-like gene from maize that regulates leaf epidermal cell identity. *Genes Devel*. *10*, 3018-3027.

O'Leary, M.H. (1981). Carbon isotope fractionation in plants. *Phytochemistry*, *20*, 553-567.

O'Leary, M.H. (1988). Carbon isotopes in photosynthesis. *Bioscience*, *38*, 328-336.

Piepho, H. P., and Möhring, J. (2007). Computing heritability and selection response from unbalanced plant breeding trials. *Genetics*, *177*, 1881-1888.

Poethig, R.S. (1990). Phase change and the regulation of shoot morphogenesis in plants. *Science*, *250*, 923-930.

Pryor, S.C., Barthelmie, R.J., and Schoof, J.T. (2013). High-resolution projections of climate-related risks for the Midwestern USA. *Climate Res.*, *56*, 61-79.

R Development Core Team, (2010). R: A language and environment for statistical computing. Vienna, Austria: R Foundation for Statistical Computing. Available at: https://www.r-project.org/.

Rebetzke, G.J., Condon, A.G., Richards, R.A., and Farquhar, G.D. (2002). Selection for reduced carbon isotope discrimination increases aerial biomass and grain yield of rainfed bread wheat. *Crop Sci.*, *42*, 739-745.

Romay, M.C., Millard, M.J., Glaubitz, J.C., Peiffer, J.A., Swarts, K.L., Casstevens, T.M., Elshire R.J., Acharya C.B., Mitchell S.E., Flint-Garcia S.A., and McMullen, M.D. (2013). Comprehensive genotyping of the USA national maize inbred seed bank. *Genome Biol.*, *14*, R55.

Saranga, Y., Jiang, C.X., Wright, R.J., Yakir, D., and Paterson, A.H. (2004). Genetic dissection of cotton physiological responses to arid conditions and their inter-relationships with productivity. *Plant Cell Environ.*, *27*, 263-277.

Teulat, B., Merah, O., Sirault, X., Borries, C., Waugh, R., and This, D. (2002). QTLs for grain carbon isotope discrimination in field-grown barley. *Theor. Appl. Genet.*, *106*, 118-126.

Tian, F., Stevens, N.M., and Buckler, E.S. (2009). Tracking footprints of maize domestication and evidence for a massive selective sweep on chromosome 10. *Proc. Nat. Acad. Sci.*, *106*, 9979-9986.

von Caemmerer, S. (2000). Biochemical models of leaf photosynthesis. CSIRO Publishing, Collingwood, Australia

von Caemmerer, S., Ghannoum, O., Pengelly, J.J., and Cousins, A.B. (2014). Carbon isotope discrimination as a tool to explore C_4 photosynthesis. *J. Exp. Bot.*, *65*, 3459-3470.

Wallace, J.G., Larsson, S.J., and Buckler, E.S. (2014). Entering the second century of maize quantitative genetics. *Heredity*, *112*, 30.

Zhang, C., Zhang, J., Zhang, H., Zhao, J., Wu, Q., Zhao, Z., and Cai, T. (2015). Mechanisms for the relationships between water-use efficiency and carbon isotope composition and specific leaf area of maize (*Zea mays* L.) under water stress. *Plant Growth Regulation*, *77*, 233-243.

CHAPTER 3

Genetic Control of Guard Cell Movement via the CO_2 Stomatal Signaling Pathway in *Zea Mays*

ABSTRACT

Stomata control the movement of CO_2 and water vapor between the atmosphere and the leaf intercellular airspace by altering the aperture size of guard cells. Stomata respond to various environmental factors such as atmospheric CO_2 levels, humidity, light, and temperature. The CO_2 stomatal signaling pathway was previously elucidated in Arabidopsis through mutant analysis of multiple genes important to the function of various steps in this pathway. The monocot pathway is thought to be similar, but not identical to the pathway found in dicot species. Here we present the characterization of *Zea mays* genetic mutants in *hlt1* (GRMZM2G028604), *opst1* (GRMZM2G138861), *opst2* (GRMZM2G171435) and *slac1* (GRMZM2G106921), genes involved in the CO_2 signaling pathway. Leaf level gas exchange measurements were used to look at the physiological response of the mutants to environmental stimuli. A single mutant of *hlt1* did not show a stomatal response phenotype, nor did an o*pst1opst2* double mutant. However, two individual mutant alleles of s*lac1* showed significant insensitivity to changes in CO_2 concentrations, resulting in a more open stomata phenotype even under high CO_2 levels. Differences in *A* rates were also observed in *slac1* mutant plants compared to WT, which was exacerbated in the *ca1ca2slac1* triple mutant. These mutants uncoupled *A* and g_s, suggesting a role for *slac1* in photosynthesis or mesophyll signaling. Dissection of the CO_2 stomatal signaling pathway will develop new insights into the optimization of stomatal regulation. Given current climate trends, the production of more efficient crops by reducing transpiration is increasing in importance for sustainable agriculture production.

INTRODUCTION

Plants uptake CO_2 through their stomatal pores for photosynthesis and simultaneously there is an efflux of water via transpiration. Precise control of CO_2 and water flux is important for maintaining a productive and efficient plant (Leakey et al., 2019). Rates of CO_2 uptake and transpirational water loss are regulated by altering the turgor pressure of guard cells, which

changes stomatal aperture (Keller et al., 1989). Stomatal aperture dynamically changes in response to environmental factors through intercellular signaling pathways (Lawson and Vialet-Chabrand, 2019). As our climate continues to change, there is uncertainty about how stomata will respond to dynamic stimuli.

Under current atmospheric conditions, stomata close in response to increasing CO_2 concentrations and open under decreasing CO_2 concentrations to maintain necessary intercellular CO_2 levels for photosynthesis (Pallas Jr, 1966). When CO_2 concentrations are high, anion channels located on the guard cell plasma membrane become activated (Vavasseur & Raghavendra, 2005). Solutes exit the guard cells resulting in a loss of turgor pressure and stomatal closure due to depolarization of the plasma membrane (Tian et al., 2015; Keller et al., 1989). This response is also reversible by the hyperpolarization of the guard cell membrane causing the activation of channels and solute uptake. Uptake results in turgor pressure increases and stomata becoming more open (Schroeder et al., 1984).

The speed and efficiency of stomatal response is thought to be influenced by anatomical, structural, and biochemical features (Lawson and Vialet-Chabrand, 2019). Stomatal size and response rate have been shown to be correlated in closely related species. Comparisons of many species has revealed that smaller stomata have quicker stomatal response rates, which has been attributed to a lower surface to volume ratio (Drake et al., 2013). Diversity in guard cell shape has also been identified as influential in determining stomatal response rates (DeMichele and Sharpe, 1973; Franks and Farquhar, 2007). Structurally, microtubules aid in controlling the shape and volume of guard cells resulting in stomatal response differences (Eisinger et al., 2012). Dicot species have bean-shaped stomata compared to the dumbbell shaped stomata present in monocots; however both stomata are composed of a pair of guard cells. Movement of solutes such as K^+ and Ca^{2+} across the plasma membrane result in stomatal aperture changes in guard cells. Therefore, stomatal responses to environmental factors are highly dependent on the rate of biochemical signaling and the speed of solute flux (Lawson and Blatt, 2014).

The biochemical mechanisms responsible for stomatal response to changes in atmospheric CO_2 concentration has been mostly studied in dicots (Tian et al., 2015; Hsu et al., 2018; Kim et al., 2010). Through mutant analysis, a biochemical pathway was constructed in *Arabidopsis thaliana*. Plasma membrane intrinsic proteins (PIPs), a family of transporters that contains

members permeable to CO_2, aid in the movement of CO_2 across the plasma membrane (Wang et al., 2016). Once CO_2 enters the guard cells, carbonic anhydrase (CA) catalyzes the hydration of CO_2 to bicarbonate (HCO_3^-) (Hu et al., 2010). Activation of RHC1 by HCO_3^- accumulation results in the binding of RHC1 to High Leaf Temperature 1 (HT1) (Tian et al. 2015). The binding of RHC1 and HT1 prevents the inhibition of protein kinases by HT1. Currently, Open Stomata 1 (OST1) and Guard Cell Hydrogen Peroxide-Resistant1 (GHR1) are known kinases functioning in this signaling pathway (Matrosova et al., 2015; Hõrak et al., 2016). As the final step of the pathway, Slow Anion Channel-Associated 1 (SLAC1) is activated by a protein kinase. SLAC1 is an S-type anion channel that pumps chloride out of the guard cells, resulting in stomatal closure.

Although a good understanding of the CO_2 signaling pathway has been achieved in dicot species, only a few studies have tried to elucidate the working CO_2 stomatal signaling pathway in monocots. Kolbe et al., found two CA proteins to have an important role in stomatal response to changing CO_2 in *Z. mays* (2018). A *slac1* mutation in *Z. mays* resulted in stomatal insensitivity to changing CO_2 levels, similar to results in *A. thaliana* (Qi et al., 2018). The *A. thaliana* OST1 ortholog in *Z. mays* (*ZmOst1*) has been shown important for ABA signaling, but its role in the CO_2 stomatal signaling pathway is currently unknown (Wu et al., 2018). Further gene characterization is necessary for the construction of a working pathway and an understanding of the genes controlling stomatal responses in *Z. mays*.

We present the characterization of genes believed to hold an important role in the CO_2 stomatal signaling pathway in *Z mays*. We discuss the characterization of *hlt1* (GRMZM2G028604), *opst1* (GRMZM2G138861), *opst2* (GRMZM2G171435) and *slac1* (GRMZM2G106921). In addition, we generate higher order mutants with *ca1* (GRMZM2G121878) and *ca2* (GRMZM2G348512), which were previously implicated in stomatal signaling.

RESULTS

Steady State Measurements

To test the putative role of each mutant in the CO_2 stomatal signaling pathway, gas exchange data was collected during a stepwise CO_2 time course. Data was logged every minute while CO_2 concentrations were held constant at 400 ppm for 30 minutes before changing to 800 ppm for 30 minutes, and then finally to 100 ppm for 60 minutes. All other environmental factors were set constant to observe stomatal response to changes in CO_2 concentrations specifically. Steady state net CO_2 assimilation (*A*) and stomatal conductance (g_s) were calculated by averaging the final 10 measurements of each genotype at each CO_2 level.

The *hlt1* gene targeted in *Z. mays* contains 81.7% protein homology with HT1 in *A thaliana* (Phytozome). The *Mu* insertion in *hlt1* was verified to be located in the first exon. Although this insertion disrupts the gene product, no significant differences in *A* or g_s steady state values were observed between *hlt1* and WT plants at any of the three CO_2 concentrations ($p > 0.05$; Table 3.1).

Of the four orthologs in *Z. mays* to the *A. thaliana* gene OST1, *Mu* insertion alleles were available in two genes (*opst1 and opst2)*, which have 85.9% and 85.4% protein homology to OST1 respectively (Phytozome). *Mu* insertions were verified to be inserted in the first exon of both *opst1* and *opst2*. When steady state data for *A* and g_s were collected for *opst1* and *opst2* single mutant plants, the only significant difference observed was in *opst1* (Table 3.1). Significantly higher g_s levels were observed at 400 ppm CO_2 in the *opst1* mutant ($p = 0.0175$; Table 3.1). Under high and low CO_2 concentrations, *opst1* also tended to have higher g_s values, but they were not significantly different from WT ($p = 0.094$ and $p = 0.071$ respectively (Table 3.1, Figure 3.2). An *opst1opst2* double mutant was also generated to explore possible functional redundancies between the gene copies. However, no significant differences were observed between *opst1opst2* and WT plants.

A single gene copy of *slac1* with 67.4% protein homology to the *A. thaliana* SLAC1 gene was found in *Z. mays* (Phytozome). There were two *Mu* insertion alleles available in *slac1, slac1-1* located in exon 1 and *slac1-2* in exon 2. Through RT-PCR and sequencing of cDNA, we determined that the *slac1-1 Mu* insertion disrupts the native transcript and produces a non-

functioning protein with a larger cDNA product compared to WT. Unlike *slac1-1*, the *slac1-2 Mu* insertion does not produce a transcript, resulting in a null allele. The *slac1-1* mutant was obtained as a homozygous stock, whereas the *slac1-2* mutant segregated wild type and homozygous mutant plants in a mendelian 1:2:1 ratio. Because of the large number of *Mu* alleles in each background, the most accurate comparison is between wild type and *slac1-2* and between the two *slac1* alleles. No steady state g_s differences were observed between the *slac1-1* and *slac1-2* mutants (Table 3.2). At 400 ppm, *slac1-2* did not have a significantly higher g_s than wild type ($p = 0.369$, Table 3.2). However, steady state measurements of g_s were significantly greater in *slac1-2* compared to WT plants at 800 ppm ($p = 0.030$, Table 3.2). Although *slac1-2* steady state g_s was lower at 100 ppm, it was not significantly different from WT ($p = 0.0919$; Figue 3.3; Table 3.2). Lower steady state *A* rates were observed in *slac1-2* mutants at 400 and 800 ppm CO_2 compared to wild type, but were not significant ($p = 0.064$ and $p = 0.095$, respectively; Figure 3.4; Table 3.2). However, at low CO_2 (100 ppm), *slac1-2* mutant plants had significantly lower steady state *A* rates compared to WT ($p = 0.01$; Table. 3.2). No steady state *A* differences were observed between the *slac1-1* and *slac1-2* mutants.

Gas exchange measurements of *ca1ca2slac1-1* triple mutant plants revealed significant g_s steady state differences (Table 3.3). Although no significant difference was observed between genotypes at 400 ppm or 100 ppm, at 800 ppm *slac1-1* and *ca1ca2slac1-1* mutants had significantly higher g_s compared to WT ($p = 0.015$ and $p = 0.002$ respectively; Table 3.3). The difference observed in the triple mutant was driven by the insensitivity of the *slac1* mutation to high CO_2 concentrations, which is highlighted by the fact that no difference was observed at 800 ppm between *slac1* single and *ca1ca2slac1* triple mutants ($p = 0.9821$; Table 3.3). Nor was there any difference in steady state g_s between *ca1ca2* double mutants and wild type ($p = 0.1383$; Table 3.3). Interestingly, significant differences in *A* were observed under all CO_2 conditions (Table 3.3; Figure 3.6). At 400 ppm *ca1ca2* had a steady state *A* that was significantly lower than WT ($p = 0.001$; Table 3.3). The *ca1ca2slac1-1* triple mutant also had significantly lower *A* compared to WT and *slac1-1* mutants ($p < 0.001$, $p = 0.01$; Table 3.3). At high CO_2 (800 ppm), *ca1ca2slac1-1* was the only mutant that showed a significantly lower *A* average when compared to WT ($p = 0.008$; Table 3.3). At 100 ppm, all four genotypes were significantly different from each other ($p < 0.05$; Table 3.3).

Stomatal Response Rates

During CO_2 concentration transitions, the rate at which stomata responded was quantified and significance was determined. The two CO_2 transitions were ambient to high concentrations (400 to 800 ppm) and high to low (800 to 100 ppm). During an increase and decrease in chamber CO_2 concentration, we would expect to observe stomatal closure and opening, respectively. A 90% threshold for opening and closing was used to test the speed of response between mutant and WT plants.

No significant difference in stomatal closure rates in response to increasing chamber CO_2 levels were observed in *hlt1 (p = 0*.519; Table 3.4A; Figure 3.1). However, on average *hlt1* was 4 seconds slower reaching 90% open in response to decreasing CO_2 ($p = 0.037$; Table 3.4A). No significant difference in stomatal response rates were observed from *opst1* and *opst2* when compared to their respective WT (Table 3.4A; Figure 3.2).

No stomatal closure response rates were calculated for *slac1-2* and WT or *slac1-1* and *slac1-2*. The severe g_s insensitivity observed in *slac1-1* and *slac1-2* prevented the accurate comparison of response rates to WT. However, due to their ability to open their stomata, opening rates were compared. The *slac1-2* mutant caused significantly slower stomatal opening rates compared to WT ($p < 0.001$; Table 3.4B; Figure 3.3). No difference in opening rates were observed between *slac1-1* and *slac1-2* ($p = 0.4669$; Table 3.4B; Figure 3.3).

For the higher order mutants, only *ca1ca2* responded to increasing CO_2 levels by closing its stomata (Figure 3.5). *ca1ca2* and WT closure rates were not significantly different ($p = 0.3136$; Table 3.4C). *slac1-1* and *ca1ca2slac1-1* showed an insensitivity to increasing CO_2 levels and closing response rates were not calculated. All mutants showed a stomatal opening response, but no significant differences were observed ($p > 0.05$; Table 3.4C)

Light Response

To observe the influence of our targeted genes on stomatal response to changes in light, leaves were adapted to dark for 30 minutes and then they were exposed to light for 30 minutes. The light source was then turned off again for 30 minutes to observe stomatal response during light to dark transition. Light response measurements were taken on *opst1opst2* double mutants and *slac1* single mutants.

In response to light, *opst1opst2* stomata opened significantly slower compared to WT (p = 0.0366; Table 3.5). During transition from light to dark, *opst1opst2* stomata closed at the same rate as WT (p = 0.183; Table 3.5). When the leaf was exposed to light, *opst1opst2* showed higher g_s and *A* values compared to WT (Figure 3.7).

The *slac1-1* mutation caused g_s to remain above 0.15 m mol $m^{-2}s^{-1}$ during dark conditions while WT was between 0.05 and 0 m mol $m^{-2}s^{-1}$ (Figure 3.8A). When the leaf was exposed to light, *slac1-1* g_s was able to rise relatively close to WT g_s, but *slac1-1* was unable to close its stomata in response to dark conditions. Rates of *A* increased quicker in *slac1-1* compared to WT. Because they maintain open stomata in the dark, there is no g_s limitation when the light is applied (Figure 3.8B).

Stomatal Density

Given the previous connection between genes involved in the stomatal signaling pathway and stomatal patterning in *A.* thaliana, stomatal density was measured in all of the mutant plants. Furthermore, stomatal density differences would contribute to differences in g_s levels observed in gas exchange measurements. No significant differences in stomatal density was observed on either the abaxial or adaxial surface of the leaf when comparing each mutant line to their corresponding WT (Figure 3.9). Therefore, the observed gas exchange differences are due to stomatal aperture and not stomatal density differences.

DISCUSSION

Characterization of *hlt1* mutant plants showed stomatal responses nearly identical to WT. Previous studies in *A. thaliana* showed a lack of stomatal response to high CO_2, and only a small hypersensitive increase under 0 ppm CO_2 (Matrosova et al. 2015, Hasimoto et al. 2006). One difference between these two species is their number of *hlt1* gene copies. *Zea mays* contains two *hlt1* paralogs. Despite targeting the gene copy with the highest homology, our results are likely due to the compensation of the non-targeted *hlt1* paralog present in *Z. mays*, which has 71.6% protein homology to HT1 (Phytozome). Further studies aim to characterize a higher order mutant targeting both *hlt1* gene copies to understand the importance of *hlt1* in *Z. mays*.

We did not find any stomatal insensitivity to changing CO_2 concentrations from *opst1, opst2,* or the *opst1opst2* double mutant. *opst1* and *opst2* are members of the SnRK2 serine/ threonine kinase family. SnRK2s have been identified in *A thaliana, O. sativa*, and *Z. mays* guard cells (Wu et al., 2018). A mutant of the *opst1* ortholog, OST1 in *A. thaliana,* impaired stomatal responses to increases and decreases in CO_2 concentrations (Xue et al, 2011; Matrosova et al, 2015). In a previous study on *Zmost1,* using the same UniformMu allele as our *opst1* resulted in ABA hyposensitivity of stomatal response (Wu et al., 2018). ZmOST1 was shown to have a similar role in ABA signaling compared to previous work with *A. thaliana ost1-1* epidermal peels (Mustilli et al., 2002). However, as a first attempt to determine a possible role of *opst1* in the *Z. mays* CO_2 signaling pathway, we did not find results consistent with *A. thaliana* characterization. We were unable to disrupt the stomatal signaling pathway in *Z. mays* with respect to changes in CO_2 concentrations. Further investigation into of the role *opst* kinases in *Z. mays* CO_2 signaling is necessary. Future work will aim at producing higher order mutants specifically targeting all four *opst* gene copies rather than just two. With only single or double mutants available, additional *opst* genes are likely compensating for the loss of *opst1* and *opst2* in our study. Alternatively, it is possible that the *opst* gene copies in *Z. mays* have subfunctionalized, given the ABA response seen in *opst1,* and that the other gene copies function exclusively in the CO_2 response pathway. Regardless, additional mutants are required to tease apart these possible scenarios.

The *slac1* loss of function alleles *slac1-1* and *slac1-2* mutants showed a general insensitivity to high CO_2 concentrations. This result is similar to previous findings in *A. thaliana*, *Oryza sativa* and *Z. mays* (Vahisalu et al,2008; Kusumi et al, 2012; Qi et al. 2018). Our results also show that *slac1-2* had significantly slower stomatal opening rates compared to WT, while also having significantly higher steady state g_s rates at 800 ppm (Table 3.4B; Table 3.2). These results confirm the importance *slac1* anion channels hold for stomatal response to changing CO_2. However, unlike previous results in Qi et al., our *slac1* mutants still opened their stomata in response to a decrease in CO_2 (2018; Figure 3.3A).

Previous studies in *Oryza sativa* found that *slac1* mutations resulted in overall higher *A* rates due to a more open stomatal phenotype compared to WT plants (Kusumi et al. 2012). Our results are not consistent with these findings and may indicate a difference between C_3 and C_4 species. Our

observations show decreases in *A* in *slac1* mutants. This effect was especially pronounced at high (800 ppm) and low (100 ppm) CO_2 concentrations (Figure 3.4). With similar g_s values, *slac1-1* and *ca1ca2 A* rates were significantly lower than WT (Figure 3.6). An even greater decrease in *A* was observed in *ca1ca2slac1-1* plants. The decrease in *A* between *ca1ca2* and *slac1* mutants and the *ca1ac2slac1-1* triple mutant appeared to be additive. The importance of *ca* for CO_2 signaling and photosynthesis have previously been reported (Studer et al., 2014 ; Kolbe et al. 2018), but the impact of *slac1* on photosynthesis has not. The *slac1* mutants uncouple *A* and g_s in that higher g_s is observed with lower *A* (Figure 3.5 and 3.6). The mechanisms and signaling cascades that control the relationship between *A* and g_s have remained unestablished (Lawson et al. 2014). Carbon sources imported from mesophyll cells could serve a role in stomatal regulation in addition to CO_2 concentrations. Sucrose, as a carbon source, was shown to possibly acts as an osmoticum for stomatal response (Azoulay-Shemer et al., 2015; Heath and Russell, 1954). Studies have also shown that stomata on epidermal peels respond to CO_2 changes most similar to WT when mesophyll tissue is present (Engineer et al., 2016). Therefore, our results suggest that *slac1* function is possibly implicated in mesophyll signaling in addition to CO_2 response.

The *slac1-1* mutant had a slightly different response in the field compared to the greenhouse grow out. While conductance rates of *slac1-1* seem to be higher under all CO_2 concentrations in the field compared to the greenhouse, the insensitivity to CO_2 change was more severe in the field. The *slac1-1* plants grown in the field also had significantly higher g_s values at 800 ppm CO_2 compared to WT. These differences could be due to differences in ambient CO_2 levels, or an increase in intensity of temperature and light in the field. However, we observed that *slac1* mutants have a slight growth phenotype in the greenhouse that was not present in field grown plants. The leaves appear notched and desiccated producing a phenotype that would be consistent with extreme water loss due to constantly open stomata. This phenotype could be the cause of decreased performance when grown under greenhouse conditions.

We observed *ca1ca2* stomatal responses similar to previous studies in *Z. mays*. The same *ca1ca2* double mutant in a previous study showed slowed stomatal response to changing CO_2 conditions (Kolbe et al., 2018). Our *ca1ca2* double mutant showed slow stomatal responses to changing CO_2 concentrations, while always maintaining a more open stomata phenotype, although not

considered significant. Our *ca1ca2slac1-1* triple mutant showed stomatal insensitivity similar to *slac1-1*. Although not considered significant, in the relative g_s graph we observe that the *ca1ca2slac1-1* triple mutant and *slac1-1* respond the same until CO_2 levels were lowered to 100 ppm. At 100 ppm CO_2, *ca1ca2slac1-1* seemed to have difficulty opening their stomata compared to the single *slac1-1* (Figure 3.5). This could be due to the reduced rates of photosynthesis, and a possible shortage of malate, which is required for normal stomatal opening.

In previous studies, a *slac1 A. thaliana* mutant resulted in higher g_s under light enviornments and a slower closure rate in response to a light to dark transition compared to WT (Vahisalu et al., 2008). Indeed, the *Z. mays slac1-1* mutants showed a lack of stomatal closure in response to a light to dark transition, however did not have a higher g_s compared to WT (Figure 3.8A). Matrosova et al., showed that *ost1-3* caused higher g_s levels in *A. thaliana* compared to WT before and after the transition from low to high intensity red and blue light (2015). We saw similar results in *opst1opst2* where g_s increases with exposure to light were significantly slow, and under light conditions *opst1opst2* showed higher g_s values compared to WT. Our findings suggest that similar to *A. thaliana*, *opst1*, *opst2*, and *slac1* likely function in stomatal control downstream of the convergence between CO_2 and light signaling pathways.

We investigated stomatal densities to determine if differences between the mutants and WT plants were due solely to stomatal aperture. In *A. thaliana*, *slac1* mutants do not show any stomatal density differences compared to WT, however *ca* mutants do show stomatal density differences when compared to WT (Vahisalu et al., 2008; Hu et al., 2010). This indicates that some aspects of the stomatal signaling pathway may affect both aperture and density. Similar to previous studies observing *Z. mays* and *O. sativa* stomatal density in *slac1* and *ca*, we observed no significant differences in stomatal density comparing each mutant to their WT background (Qi et al., 2018; Kolbe et al., 2018; Chen et al., 2017) . Therefore, the differences in g_s steady states and speed of stomatal responses in our mutants are not due to stomatal density.

MATERIALS AND METHODS

All UniformMu insertion lines were acquired from the USDA Maize Genetic Stock Center located at the University of Illinois (Portwood et al., 2018). The characterized mutants include

hlt1 (insert mu1061469 in stock UFMu 07970), *opst1* (insert mu1008082 in stock UFMu 00741), *opst2* (insert mu1092021 in stock UFMu 11151), *slac1-1* (insert mu1013891 in stock UFMu 01251), and *slac1-2* (insert mu1037824 in stock UFMu 04043). It is important to note that *opst1* is also referred to as *snrkII8* in previous publications. Segregating seed was planted in the greenhouse and field for multiple generations between 2016 and 2019 to obtain homozygous seed stocks and to generate higher order mutants. Homozygous stocks of each *Mu* and their corresponding wild-type W22 background were attained, and seeds were planted for gas exchange measurements. Genetic screens were used to produce non-segregating *Mu* stocks. Tissue was collected from week old seedlings and immediately placed in liquid nitrogen. DNA extractions were done following a CTAB protocol as described in (Kolbe et al., 2018). Forward and reverse primers were designed to flank the expected location of each transposable element insertion. A *Mu* specific primer AJS516 (GCCTCYATTTCGTCGAATCCS) was designed to align with the inverted terminal repeats located on each end of the transposable element (Settles et al., 2004). *Mu* insertions were confirmed using genic-genic and genic-mutator primer sets with a Phire Hot Start II (#F-122L) or Gotaq Flexi (# M829B) PCR reaction following manufacturers recommendations. Insertion placement of the transposable elements was also confirmed in mutants using Sanger sequencing at the Roy J. Carver Biotechnology Center at the University of Illinois.

Plant Growth

Greenhouse grown plants were planted in 50 well plug trays (T.O. Plastics #720568C) with a 1:1 mixture of Sun Gro Sunshine LC1 and a general purpose 1:1:1 – soil : peat : perlite mix with 5 pounds of dolomitic lime, 2 pounds of 0-46-0, 3 pounds of gypsum, and 2 pounds of Epsom per yard. During the first two weeks of plant growth, leaf tissue was collected for genotyping as described above. Plants remained in flats for 2 weeks and then were transplanted into a greenhouse ground bed. Plants were fertilized with 15-5-15 CalMag at a concentration of 300 ppm weekly and Sprint 330 chelated iron was applied once to all plants. Gas exchange measurements were taken on the uppermost fully expanded leaf between V9 - V11 and plants were grown to maturity if seed was needed.

Field plots were planted in 2017 and 2018 at the Crop Sciences Research and Education Center at the University of Illinois (40.091015, -88.228104). Nitrogen was applied before planting at a

rate of 90 lbs per acre. Leaf tissue was collected from seedlings 2-3 weeks after planting as necessary for genotyping as described above. Gas exchange measurements started when all plants were at least V9. Light response was measured on all plants at V13 after CO_2 response measurements.

Gas Exchange

All gas exchange measurements were taken using a Li-6800 gas exchange system with a 3 x 3cm chamber with an LED light source. Chamber temperature was set constant at 25°C during greenhouse measurements and 29°C for field measurements. Humidity was controlled to maintain a leaf VPD of 1.5 kPa. Light was set constant at 1,500 µmol m^{-2} s^{-1} for greenhouse measurements or 2,000 µmol m^{-2} s^{-1} for field measurements. The number of plants measured as biological replicates varied for each genotype (*hlt1* n = 3, *opst1* and *opst2* n = 5 and *slac1* n = 4).

Gas exchange measurements started 1 hour after artificial light turned on in the greenhouse or after daybreak in the field, and ended by 14:00 same day. For each plant measured, the leaf was clamped and remained under constant conditions at 400 ppm CO_2 for at least 30 minutes. When steady state was achieved, data collection began and a measurement was taken every minute throughout the time course. Data points were logged at 400 ppm CO_2 for 30 minutes. Then the CO_2 concentration of the chamber was increased to 800 ppm and data points were logged for 30 minutes allowing the observation of stomatal closure rates and steady state values under a high CO_2 concentration. The final CO_2 change was a decrease to 100 ppm to observe stomatal opening rates. Data points were logged for 1 hour at 100 ppm CO_2 due to a longer acclimation time necessary to reach steady state values.

To measure light response, all environmental factors remained constant as described above in the CO_2 stepwise responses. The CO_2 concentration was held constant in the chamber at 400 ppm. After clamping, the leaf was exposed to 30 minutes at 0 µmol m^{-2} s^{-1} and was allowed to reach steady state. Light was then increased to 1,500 µmol m^{-2} s^{-1} or 2,000 µmol m^{-2} s^{-1} in the greenhouse and field, respectively and maintained for 30 minutes to observe stomatal response to light induction. Light intensity was then returned to 0 µmol m^{-2} s^{-1} for 30 minutes to complete the stepwise protocol.

Statistical Analyses

A one way ANOVA or T-test was used to determine significant steady state genotype differences using the last 10 data points at each CO_2 concentration (400, 800, and 100 ppm). To determine the rate of stomatal opening and closing, in response to changing CO_2 concentration, the time necessary to reach 90% open or closed was calculated as done by (Leakey et al., 2005 and Kolbe et al., 2018). The starting value was determined to be the final conductance measurement before the change in CO_2 occurred. The steady state open/closed response value was determined by averaging the final 10 points for each CO_2 concentration. The total time it took stomata to pass 90% open/closed was used to run one-way ANOVAs and Tukey's posthoc tests to determine significant differences in total time to 90% open/closed between mutants and WT.

Stomatal Densities

Three tissue samples (5 x 3cm) were collected for each plant from the same location on the leaf as gas exchange measurements. Samples were immediately placed in liquid nitrogen then transferred to a -80°C freezer. Leaf samples were thawed and placed on microscope slides using double sided tape before imaging. A Nano Focus µsurf confocal 3D scanner was used to image the abaxial and adaxial sides of the leaf surface at 20x magnification. Total number of stomata were counted in each 3 x 3mm image. Three images were taken on each side of leaf sample. Technical reps (n = 3) for each plant were averaged and a T-test determined if any significant differences in stomatal density were present comparing each mutant to their W22 WT background.

FIGURES AND TABLES

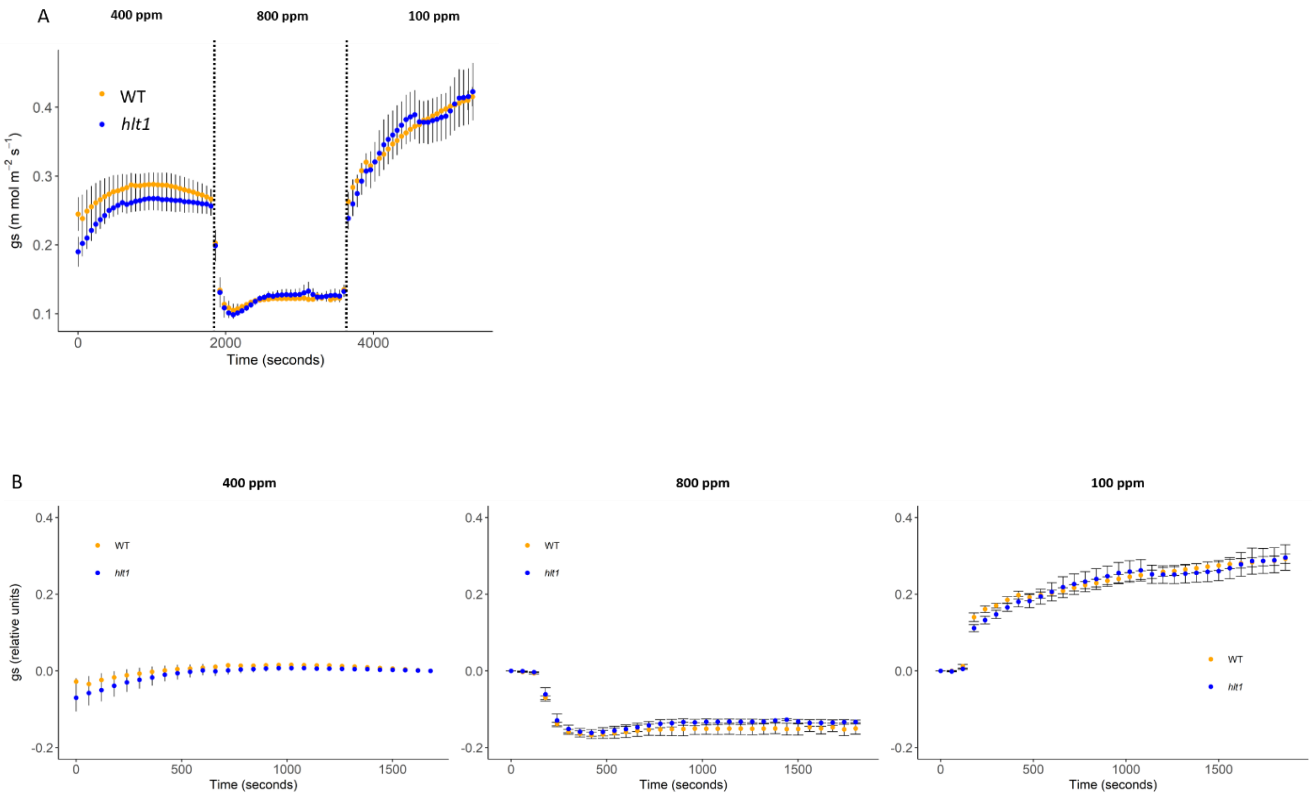

Figure 3.1: *hlt1* response to varying CO_2

(A) Average g_s level ± standard error at one minute intervals for *hlt1* (blue) and WT (orange) during three different CO_2 concentrations. Vertical dashed lines indicate change in CO_2 concentration, and CO_2 concentration is listed at the top of the graph. (B) Average g_s ± standard error is normalized to the final point collected during the previous CO_2 concentration. Initial steady state values are normalized to the final 400 ppm data point.

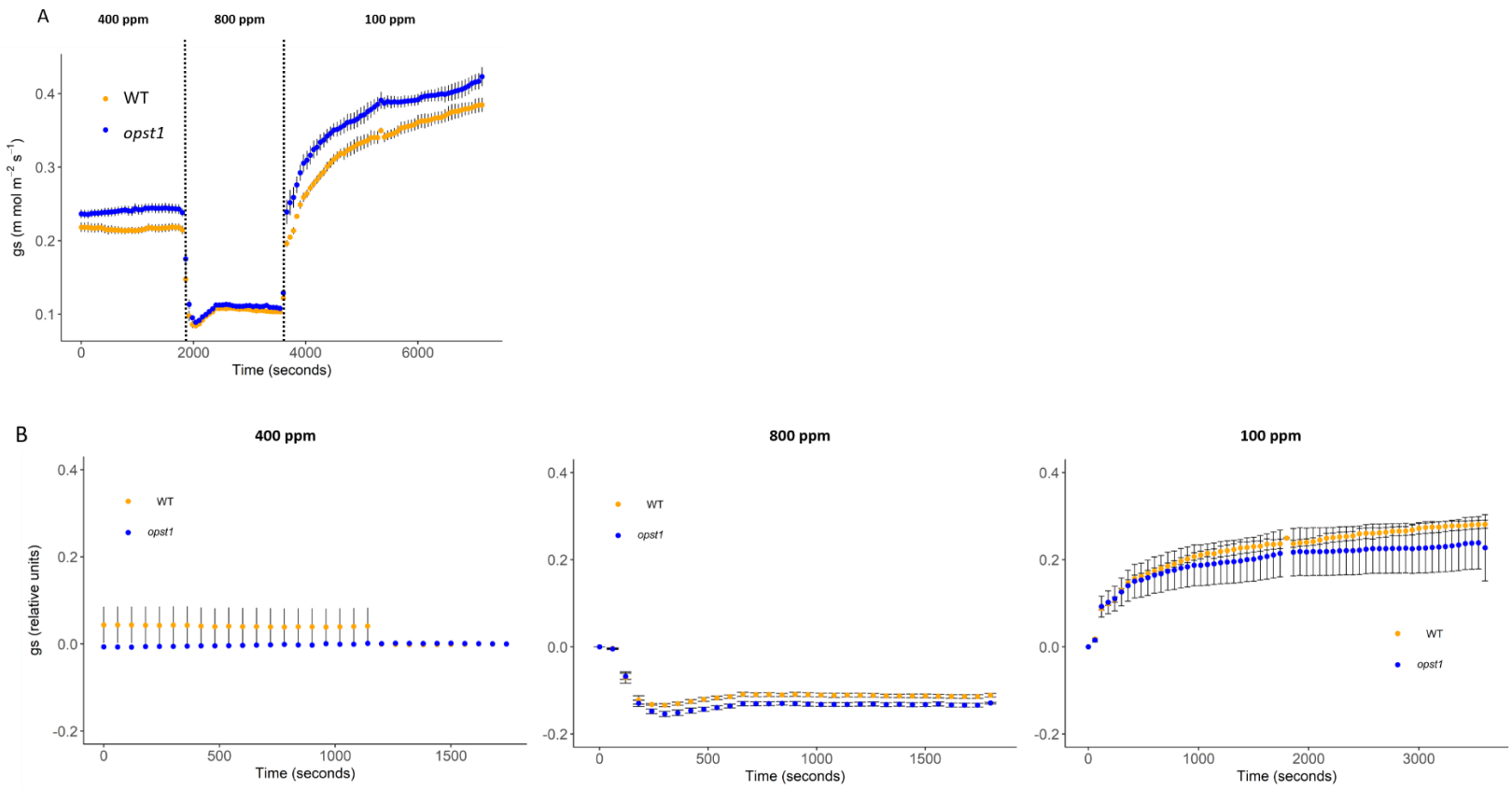

Figure 3.2: *opst1* response to varying CO_2

(A) Average g_s level ± standard error at one minute intervals for *opst1* (blue) and WT (orange) during three different CO_2 concentrations. Vertical dashed lines indicate change in CO_2 concentration, and CO_2 concentration is listed at the top of the graph. (B) Average g_s ± standard error is normalized to the final point collected during the previous CO_2 concentration. Initial steady state values are normalized to the final 400 ppm data point.

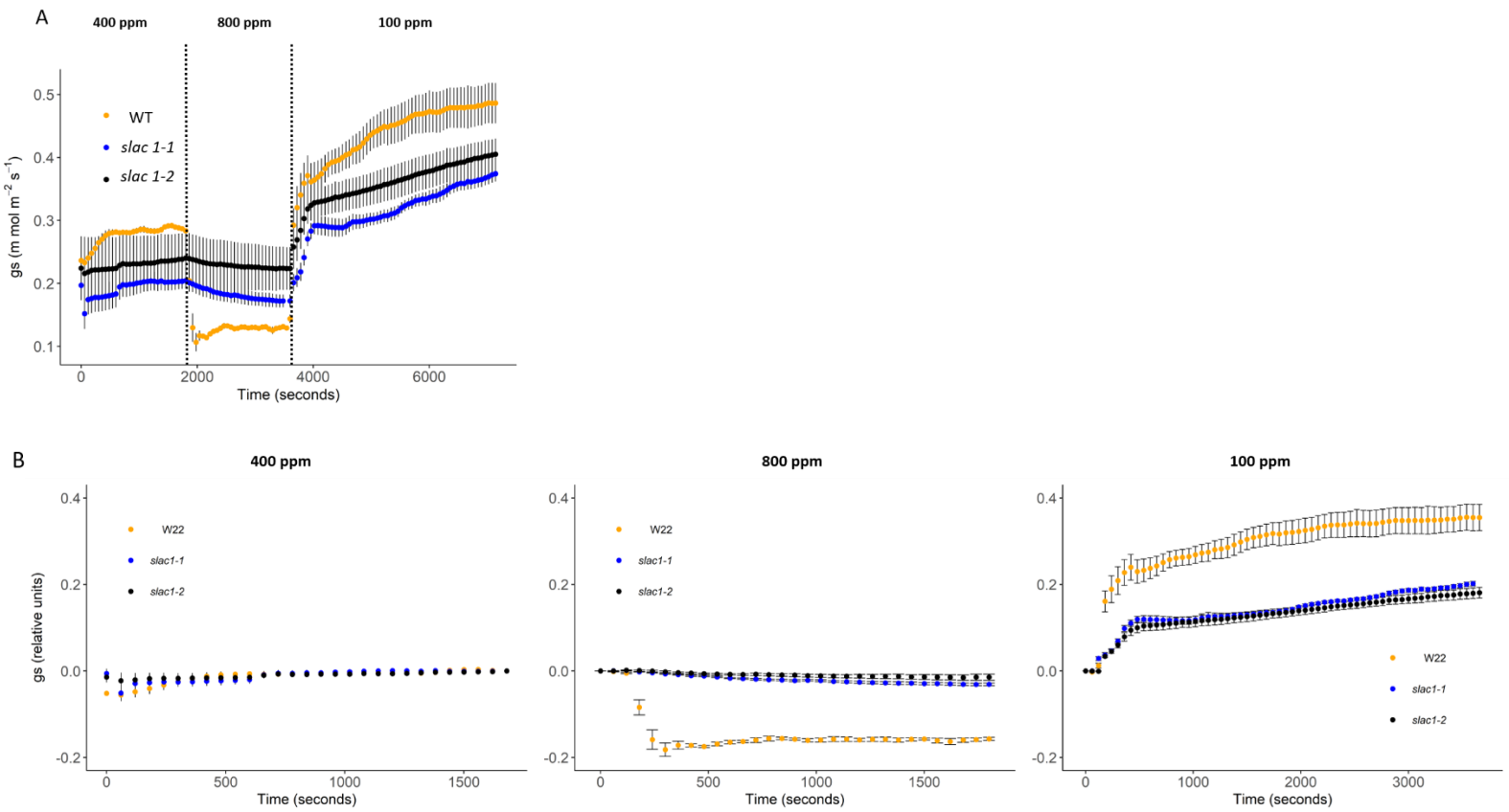

Figure 3.3: *slac1* response to varying CO_2

(A) Average g_s level ± standard error at one minute intervals for *slac1-1* (blue), *slac1-2* (black) and WT (orange) during three different CO_2 concentrations. Vertical dashed lines indicate change in CO_2 concentration, and CO_2 concentration is listed at the top of the graph. (B) Average g_s ± standard error is normalized to the final point collected during the previous CO_2 concentration. Initial steady state values are normalized to the final 400 ppm data point.

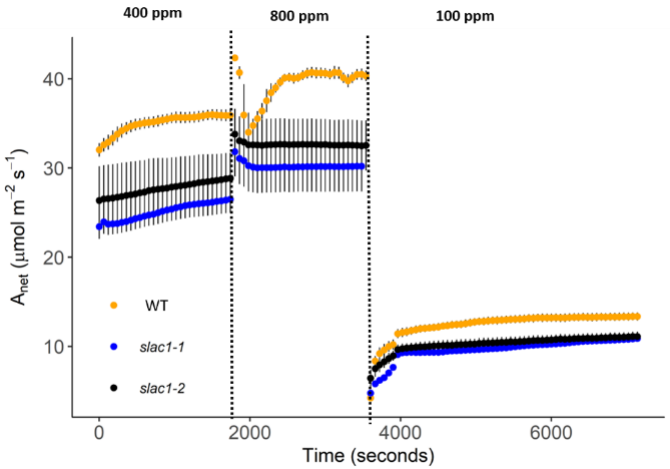

Figure 3.4: *slac1* carbon assimilation rates at varying CO_2 concentrations

Average *A* level ± standard error at one minute intervals for *slac1-1* (blue), *slac1-2* (black), and WT (orange) during three different CO_2 concentrations. Vertical dashed lines indicate change in CO_2 concentration, and CO_2 concentration is listed at the top of the graph.

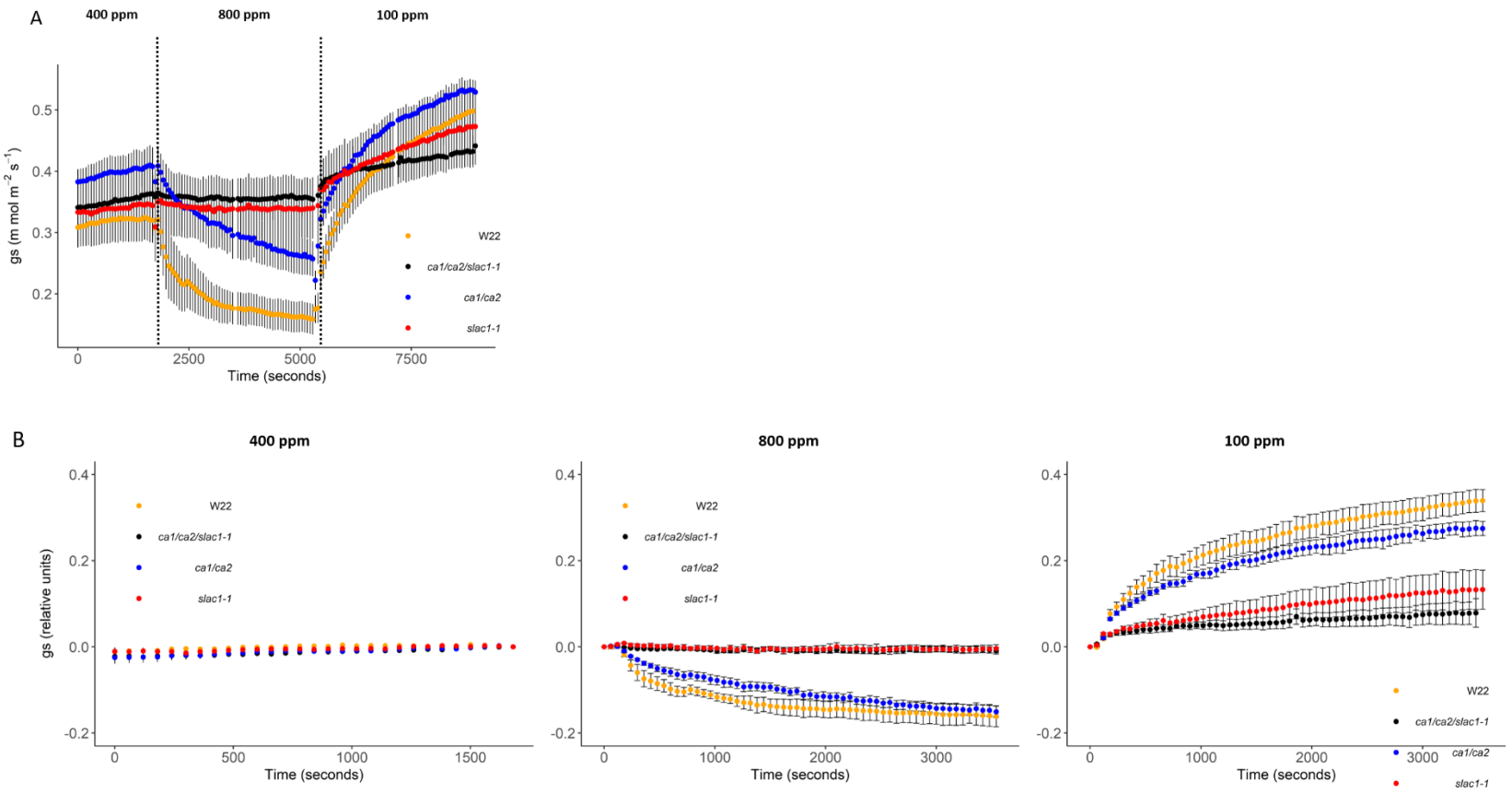

Figure 3.5: *ca1ca2slac1-1* response to varying CO_2

(A) Average g_s level ± standard error at one minute intervals for *slac1-1* (red), *ca1ca2* (blue), *ca1ca2slac1-1* (black), and WT (orange) during three different CO_2 concentrations. Vertical dashed lines indicate change in CO_2 concentration, and CO_2 concentration is listed at the top of the graph. (B) Average g_s ± standard error is normalized to the final point collected during the previous CO_2 concentration. Initial steady state values are normalized to the final 400 ppm data point.

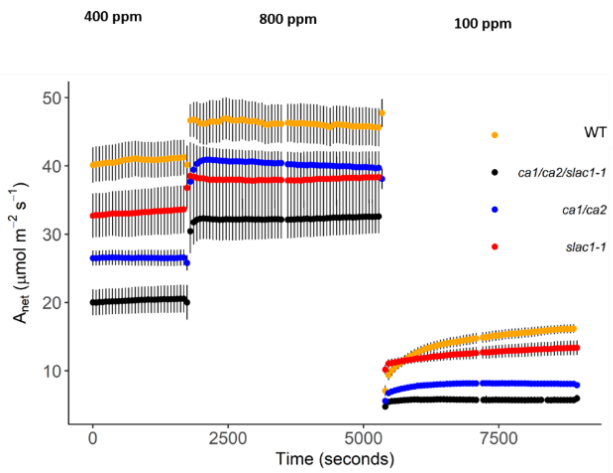

Figure 3.6: *ca1ca2slac1-1* carbon assimilation rates at varying CO_2 concentrations

(A) Average g_s level ± standard error at one minute intervals for *slac1-1* (red), *ca1ca2* (blue), *ca1ca2slac1-1* (black), and WT (orange) during three different CO_2 concentrations. Vertical dashed lines indicate change in CO_2 concentration, and CO_2 concentration is listed at the top of the graph. (B) Average g_s ± standard error is normalized to the final point collected during the initial 400 ppm CO_2 concentration.

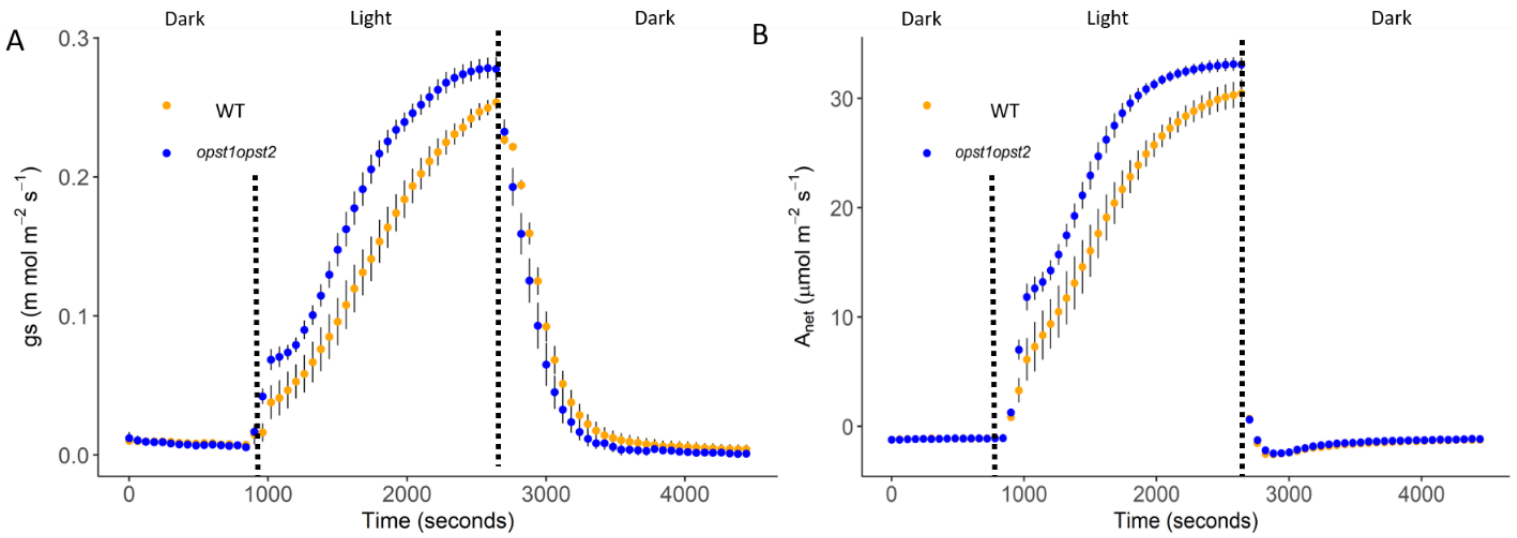

Figure 3.7: *opst1opst2* light response

(A) Average g_s level ± standard error at one minute intervals for *opst1opst2* (blue) and WT (orange) during light and dark environments. Vertical dashed lines indicate change in light intensity, and dark (0 m mol $m^{-2}s^{-1}$) or light (2000 m mol $m^{-2}s^{-1}$) is listed above the graph. (B) Average A ± standard error at one minute intervals.

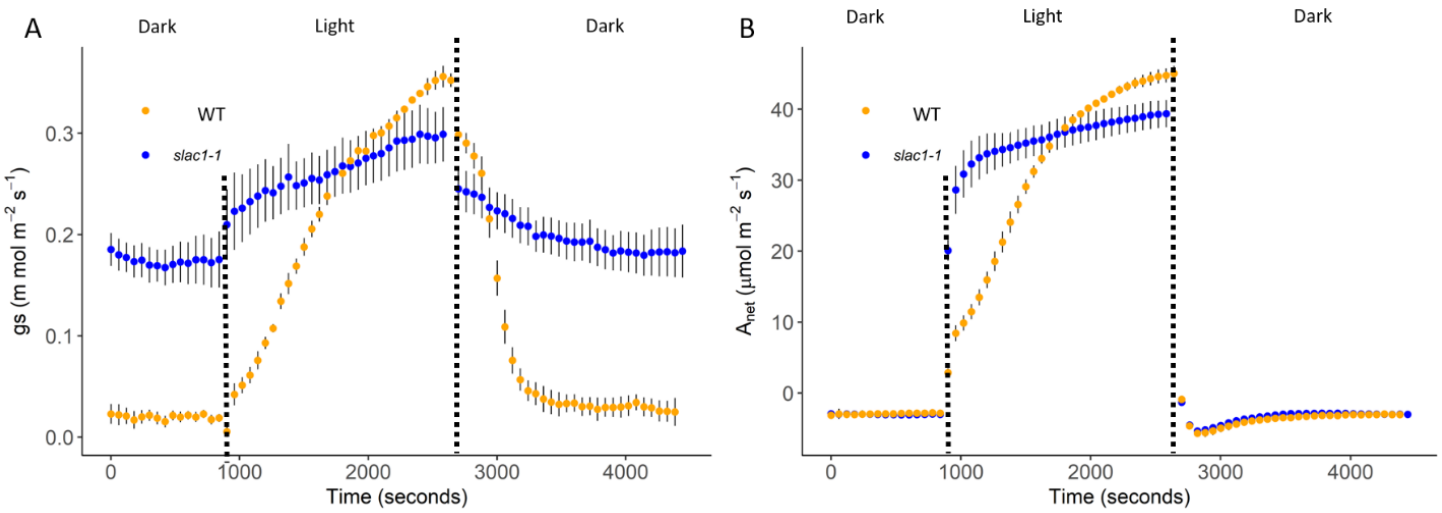

Figure 3.8: *slac1-1* light response

(A) Average g_s level ± standard error at one minute intervals for *slac1-1* (blue) and WT (orange) during light and dark environments. Vertical dashed lines indicate change in light intensity, and dark (0 m mol $m^{-2}s^{-1}$) or light (2000 m mol $m^{-2}s^{-1}$) is listed above the graph. (B) Average *A* ± standard error at one minute intervals.

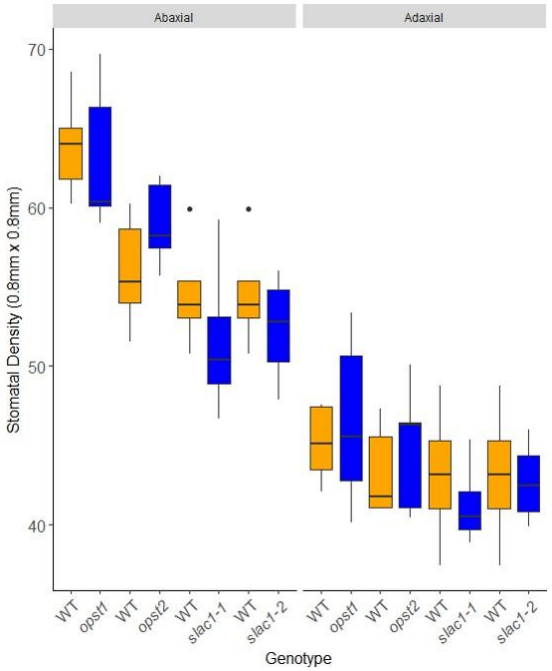

Figure 3.9: Stomatal density

The genotype corresponding to each boxplot is presented on the x-axis. The boxplots show stomatal density for biological replicates. The box shows the first and third quartiles and the horizontal line represents the mean. Whiskers represent mild outliers and open circles represent extreme outliers.

Table 3.1 Steady state values
Data are presented as averages ± standard error. Values represent the average of the final 10 g_s or A data points at each CO_2 concentration.

	Stomatal conductance (g_s) mol m^{-2} s^{-1}			Net Photosynthesis (A) µmol m^{-2} s^{-1}		
	400 ppm[‡]	800 ppm[†]	100 ppm[†]	400 ppm[†]	800 ppm[†]	100 ppm[†]
hlt1	0.263 ± 0.016	0.127 ± 0.009	0.400 ± 0.037	0.263 ± 0.016	0.127 ± 0.009	12.18 ± 0.75
WT	0.281 ± 0.018	0.123 ± 0.004	0.402 ± 0.014	0.281 ± 0.018	0.123 ± 0.004	11.89 ± 0.21
opst1	0.244 ± 0.007[a]	0.110 ± 0.003	0.409 ± 0.011	0.244 ± 0.007	0.110 ± 0.003	13.38 ± 0.41
WT	0.218 ± 0.005[b]	0.105 ± 0.002	0.373 ± 0.008	0.218 ± 0.005	0.105 ± 0.002	12.63 ± 0.3
opst2	0.251 ± 0.008	0.118 ± 0.002	0.452 ± 0.018	0.251 ± 0.008	0.118 ± 0.002	14.49 ± 0.45
WT	0.258 ± 0.009	0.118 ± 0.002	0.429 ± 0.014	0.258 ± 0.009	0.118 ± 0.002	14.17 ± 0.34

[†]No significant differences were observed

[‡]Letters represent significant differences between genotypes

Table 3.2 Steady state values
Data are presented as averages ± standard error. Values represent the average of the final 10 g_s or A data points at each CO_2 concentration.

	Stomatal conductance (g_s) mol m^{-2} s^{-1}			Net Photosynthesis (A) µmol m^{-2} s^{-1}		
	400 ppm[†]	800 ppm[‡]	100 ppm[‡]	400 ppm[‡]	800 ppm[‡]	100 ppm[‡]
slac1-1	0.203 ± 0.014	0.174 ±0.011[ab]	0.366 ± 0.012[b]	26.09 ± 1.44[a]	30.18 ± 2.82[a]	10.75 ± 0.26[b]
slac1-2	0.235 ± 0.042	0.225 ± 0.036[b]	0.400 ± 0.025[a]	28.44 ± 3.07[ab]	32.57 ± 2.85[ab]	11.03 ± 0.53[b]
WT	0.287 ± 0.002	0.129 ± 0.003[a]	0.483 ± 0.032[a]	35.84 ± 0.61[b]	40.43 ± 0.56[b]	13.32 ± 0.44[a]

[†]No significant differences were observed

[‡]Letters represent significant differences between genotypes

Table 3.3 Steady state values
Data are presented as averages ± standard error. Values represent the average of the final 10 g_s or A data points at each CO_2 concentration.

	Stomatal conductance (g_s) mol m^{-2} s^{-1}			Net Photosynthesis (A) µmol m^{-2} s^{-1}		
	400 ppm[†]	800 ppm[‡]	100 ppm[†]	400 ppm[‡]	800 ppm[‡]	100 ppm[‡]
ca1ca2	0.405 ± 0.030	0.262 ±0.030[ab]	0.530 ± 0.018	26.53 ± 1.18[bc]	39.81 ± 1.33[ab]	8.10 ± 0.37[d]
slac1-1	0.345 ± 0.044	0.339 ± 0.041[b]	0.469 ± 0.053	33.49 ± 3.03[ab]	38.31 ± 3.29[ab]	13.30 ± 0.91[c]
ca1ca2slac1-1	0.359 ± 0.036	0.357 ± 0.032[b]	0.431 ± 0.025	20.50 ± 2[c]	32.55 ± 2.52[b]	5.714 ± 0.48[b]
WT	0.322 ± 0.037	0.162 ± 0.025[a]	0.490 ± 0.030	41.07 ± 2.61[a]	45.77 ± 2.77[a]	16.06 ± 0.65[a]

[†]No significant differences were observed

[‡]Letters represent significant differences between genotypes

Table 3.4A Stomatal response rates
Data presented as averages (minutes) ± standard error.

Genotype	CO_2 Close[†]	CO_2 Open[‡]
hlt1	4.7 ± 0.3	16 ± 0.6[a]
WT	4.3 ± 0.3	20 ± 1[b]
opst1	13.2 ± 0.2	28.2 ± 1.8
WT	13.2 ± 0.2	33.2 ± 2.6
opst2	2.2 ± 0.2	26 ± 1.9
WT	3 ± 0.5	29.6 ± 2.4

Table 3.4B Stomatal response rates
Data presented as averages (minutes) ± standard error.

	CO_2 Close[†]	CO_2 Open[‡]
slac1-1	NA	46.3 ± 0.5[b]
slac1-2	NA	44.5 ± 0.6[b]
WT	NA	30.3 ± 1.5[a]

Table 3.4C Stomatal response rates
Data presented as averages (minutes) ± standard error.

Genotype	CO_2 Close[†]	CO_2 Open[†]
ca1ca2	36.4 ± 4.9	40.8 ± 2.2
slac1-1	NA	44.7 ± 0.3
ca1ca2slac1-1	NA	31.2 ± 8.3
WT	23.2 ± 6.1	39.8 ± 1.5

[†]No significant differences were observed

[‡]Letters represent significant differences between genotypes

Table 3.5 Stomatal response rates
Data presented as averages (minutes) ± standard error.

Genotype	PAR Close[†]	PAR Open[‡]
slac1-1	16 ± 2.6	16.3 ± 3.7
WT	9.3 ± 0.3	20.7 ± 0.9
opst1opst2	9.6 ± 0.8	19.4 ± 0.9[a]
WT	11.2 ± 0.7	22.2 ± 0.5[b]

[†]No significant differences were observed

[‡]Letters represent significant differences between genotypes

REFERENCES

Azoulay-Shemer, T., Bagheri, A., Wang, C., Palomares, A., Stephan, A. B., Kunz, H. H., & Schroeder, J. I. (2016). Starch biosynthesis in guard cells but not in mesophyll cells is involved in CO_2-induced stomatal closing. *Plant physiology*, *171*(2), 788-798.

Chen, T., Wu, H., Wu, J., Fan, X., Li, X., & Lin, Y. (2017). Absence of OsβCA1 causes a CO2 deficit and affects leaf photosynthesis and the stomatal response to CO2 in rice. *The Plant Journal*, *90*(2), 344-357.

DeMichele, D. W., & Sharpe, P. J. (1973). An analysis of the mechanics of guard cell motion. *Journal of Theoretical Biology*, *41*(1), 77-96.

Drake, P. L., Froend, R. H., & Franks, P. J. (2013). Smaller, faster stomata: scaling of stomatal size, rate of response, and stomatal conductance. *Journal of experimental botany*, *64*(2), 495-505.

Ehleringer, J., & Björkman, O. (1977). Quantum yields for CO_2 uptake in C_3 and C_4 plants: dependence on temperature, CO_2, and O_2 concentration. *Plant Physiology*, *59*(1), 86-90.

Eisinger, W. R., Kirik, V., Lewis, C., Ehrhardt, D. W., & Briggs, W. R. (2012). Quantitative changes in microtubule distribution correlate with guard cell function in Arabidopsis. *Molecular plant*, *5*(3), 716-725.

Engineer, C. B., Hashimoto-Sugimoto, M., Negi, J., Israelsson-Nordström, M., Azoulay-Shemer, T., Rappel, W. J., Iba, K., & Schroeder, J. I. (2016). CO2 sensing and CO2 regulation of stomatal conductance: advances and open questions. *Trends in Plant Science*, *21*(1), 16-30.

Franks, P. J., & Farquhar, G. D. (2007). The mechanical diversity of stomata and its significance in gas-exchange control. *Plant physiology*, *143*(1), 78-87.

Grantz, D. A. (1990). Plant response to atmospheric humidity. *Plant, Cell & Environment*, *13*(7), 667-679.

Hashimoto, M., Negi, J., Young, J., Israelsson, M., Schroeder, J. I., & Iba, K. (2006). Arabidopsis HT1 kinase controls stomatal movements in response to CO 2. *Nature cell biology*, *8*(4), 391.

Heath, O. V. S., & Russell, J. (1954). Studies in Stomatal Behaviour: VI. AN INVESTIGATION OF THE LIGHT RESPONSES OF WHEAT STOMATA WITH THE ATTEMPTED ELIMINATION OF CONTROL BY THE MESOPHYLL. *Journal of Experimental Botany*, *5*(2), 269-292.

Hõrak, H., Sierla, M., Tõldsepp, K., Wang, C., Wang, Y. S., Nuhkat, M., Valk, E., Pechter, P., Merilo, E., Salojärvi, J., Overmyer, K., Loog, M., Brosché, M., Schroeder, J.I., Kangasjärvi, J., & Kollist, H. (2016). A dominant mutation in the HT1 kinase uncovers roles of MAP kinases and GHR1 in CO2-induced stomatal closure. *The Plant Cell*, *28*(10), 2493-2509.

Hsu, P. K., Takahashi, Y., Munemasa, S., Merilo, E., Laanemets, K., Waadt, R., Pater, D., Kollist, H., & Schroeder, J. I. (2018). Abscisic acid-independent stomatal CO2 signal transduction pathway and convergence of CO2 and ABA signaling downstream of OST1 kinase. *Proceedings of the National Academy of Sciences*, *115*(42), E9971-E9980.

Hu, H., Boisson-Dernier, A., Israelsson-Nordström, M., Böhmer, M., Xue, S., Ries, A., Godoski, J., Kuhn, J.M., & Schroeder, J. I. (2010). Carbonic anhydrases are upstream regulators of CO 2-controlled stomatal movements in guard cells. *Nature cell biology*, *12*(1), 87.

Keller, B. U., Hedrich, R., & Raschke, K. (1989). Voltage-dependent anion channels in the plasma membrane of guard cells. *Nature*, *341*(6241), 450.

Kim, T. H., Böhmer, M., Hu, H., Nishimura, N., & Schroeder, J. I. (2010). Guard cell signal transduction network: advances in understanding abscisic acid, CO2, and Ca2+ signaling. *Annual review of plant biology*, *61*, 561-591.

Kinoshita, T., Doi, M., Suetsugu, N., Kagawa, T., Wada, M., & Shimazaki, K. I. (2001). Phot1 and phot2 mediate blue light regulation of stomatal opening. *Nature*, *414*(6864), 656.

Kolbe, A. R., Brutnell, T. P., Cousins, A. B., & Studer, A. J. (2018). Carbonic anhydrase mutants in Zea mays have altered stomatal responses to environmental signals. *Plant Physiology*, *177*(3), 980-989.

Kolbe, A. R., Studer, A. J., Cornejo, O. E., & Cousins, A. B. (2019). Insights from transcriptome profiling on the non-photosynthetic and stomatal signaling response of maize carbonic anhydrase mutants to low CO 2. *BMC genomics*, *20*(1), 138.

Kusumi, K., Hirotsuka, S., Kumamaru, T., & Iba, K. (2012). Increased leaf photosynthesis caused by elevated stomatal conductance in a rice mutant deficient in SLAC1, a guard cell anion channel protein. *Journal of Experimental Botany*, *63*(15), 5635-5644.

Lawson, T., & Blatt, M. R. (2014). Stomatal size, speed, and responsiveness impact on photosynthesis and water use efficiency. *Plant physiology*, *164*(4), 1556-1570.

Lawson, T., Simkin, A. J., Kelly, G., & Granot, D. (2014). Mesophyll photosynthesis and guard cell metabolism impacts on stomatal behaviour. *New Phytologist*, *203*(4), 1064-1081.

Lawson, T., & Vialet-Chabrand, S. (2019). Speedy stomata, photosynthesis and plant water use efficiency. *New Phytologist*, *221*(1), 93-98.

Lawson, T., von Caemmerer, S., & Baroli, I. (2010). Photosynthesis and stomatal behaviour. In *Progress in botany 72* (pp. 265-304). Springer, Berlin, Heidelberg.

Leakey, A. D. B., Scholes, J. D., & Press, M. C. (2004). Physiological and ecological significance of sunflecks for dipterocarp seedlings. *Journal of Experimental Botany*, *56*(411), 469-482.

Leakey, A. D., Ferguson, J. N., Pignon, C. P., Wu, A., Jin, Z., Hammer, G. L., & Lobell, D. B. (2019). Water Use Efficiency as a Constraint and Target for Improving the Resilience and Productivity of C3 and C4 Crops. *Annual review of plant biology*, *70*, 781-808.

Matrosova, A., Bogireddi, H., Mateo-Peñas, A., Hashimoto-Sugimoto, M., Iba, K., Schroeder, J. I., & Israelsson-Nordström, M. (2015). The HT1 protein kinase is essential for red light-induced stomatal opening and genetically interacts with OST1 in red light and CO2-induced stomatal movement responses. *New Phytologist*, *208*(4), 1126-1137.

McAusland, L., Vialet-Chabrand, S., Davey, P., Baker, N. R., Brendel, O., & Lawson, T. (2016). Effects of kinetics of light-induced stomatal responses on photosynthesis and water-use efficiency. *New Phytologist*, *211*(4), 1209-1220.

Mustilli, A. C., Merlot, S., Vavasseur, A., Fenzi, F., & Giraudat, J. (2002). Arabidopsis OST1 protein kinase mediates the regulation of stomatal aperture by abscisic acid and acts upstream of reactive oxygen species production. *The Plant Cell*, *14*(12), 3089-3099.

Negi, J., Matsuda, O., Nagasawa, T., Oba, Y., Takahashi, H., Kawai-Yamada, M., Uchimiya, H., Hashimoto, M., & Iba, K. (2008). CO 2 regulator SLAC1 and its homologues are essential for anion homeostasis in plant cells. *Nature*, *452*(7186), 483.

Pallas Jr, J. E. (1966). Mechanisms of guard cell action. *The Quarterly review of biology*, *41*(4), 365-383.

Portwood JL II, Woodhouse MR, Cannon EK, Gardiner JM, Harper LC, Schaeffer ML, Walsh JR, Sen TZ, Cho KT, Schott DA, Braun BL, Dietze M, Dunfee B, Elsik CG, Manchanda N, Coe E, Sachs M, Stinard P, Tolbert J, Zimmerman S, Andorf CM. MaizeGDB 2018: the maize multi-genome genetics and genomics database. Nucleic Acids Res. 2018 Nov 8. doi: 10.1093/nar/gky1046

Qi, G. N., Yao, F. Y., Ren, H. M., Sun, S. J., Tan, Y. Q., Zhang, Z. C., Qiu, B.S., & Wang, Y. F. (2018). The S-Type Anion Channel ZmSLAC1 Plays Essential Roles in Stomatal Closure by Mediating Nitrate Efflux in Maize. *Plant and Cell Physiology*, *59*(3), 614-623.

Schroeder, J. I., Hedrich, R., & Fernandez, J. M. (1984). Potassium-selective single channels in guard cell protoplasts of Vicia faba. *Nature*, *312*(5992), 361.

Schulze, E. D., Lange, O. L., Kappen, L., Buschbom, U., & Evenari, M. (1973). Stomatal responses to changes in temperature at increasing water stress. *Planta*, *110*(1), 29-42.

Settles, A. M., Latshaw, S., & McCarty, D. R. (2004). Molecular analysis of high-copy insertion sites in maize. *Nucleic acids research*, *32*(6), e54-e54.

Studer, A. J., Gandin, A., Kolbe, A. R., Wang, L., Cousins, A. B., & Brutnell, T. P. (2014). A limited role for carbonic anhydrase in C4 photosynthesis as revealed by a ca1ca2 double mutant in maize. *Plant physiology*, *165*(2), 608-617.

Teng, N., Wang, J., Chen, T., Wu, X., Wang, Y., & Lin, J. (2006). Elevated CO2 induces physiological, biochemical and structural changes in leaves of Arabidopsis thaliana. *New Phytologist*, *172*(1), 92-103.

Tian, W., Hou, C., Ren, Z., Pan, Y., Jia, J., Zhang, H., Bai, F., Zhang, P., Zhu, H., He, Y., Luo, S., Li, L., Luan, S. (2015). A molecular pathway for CO 2 response in Arabidopsis guard cells. *Nature Communications*, *6*, 6057.

Twohey III, R. J., Roberts, L. M., & Studer, A. J. (2019). Leaf stable carbon isotope composition reflects transpiration efficiency in Zea mays. *The Plant Journal*, *97*(3), 475-484.

Vahisalu, T., Kollist, H., Wang, Y. F., Nishimura, N., Chan, W. Y., Valerio, G., Lamminmäki, A., Brosché, M., Moldau, H., Desikan, R., Schroeder, J. I., & Kangasjärvi, J. (2008). SLAC1 is required for plant guard cell S-type anion channel function in stomatal signaling. *Nature*, *452*(7186), 487.

Vavasseur, A., & Raghavendra, A. S. (2005). Guard cell metabolism and CO2 sensing. *New Phytologist*, *165*(3), 665-682.

Wang, C., Hu, H., Qin, X., Zeise, B., Xu, D., Rappel, W. J., Boron, W. F., & Schroeder, J. I. (2016). Reconstitution of CO2 regulation of SLAC1 anion channel and function of CO2-permeable PIP2; 1 aquaporin as CARBONIC ANHYDRASE4 interactor. *The Plant Cell*, *28*(2), 568-582.

Wu, Q., Wang, M., Shen, J., Chen, D., Zheng, Y., & Zhang, W. (2018). ZmOST1 mediates abscisic acid regulation of guard cell ion channels and drought stress responses. *Journal of integrative plant biology*.

Xue, S., Hu, H., Ries, A., Merilo, E., Kollist, H., & Schroeder, J. I. (2011). Central functions of bicarbonate in S-type anion channel activation and OST1 protein kinase in CO2 signal transduction in guard cell. *The EMBO journal*, *30*(8), 1645-1658

CHAPTER 4

Conclusion

The research described here combines both field and greenhouse measured plants using a variety of techniques. In addition, this research engages both the scientific disciplines of genetics and physiology. Through an interdisciplinary approach, leaf traits related to water use in *Zea mays* were studied. This research gives me a unique perspective on plant water use and how improvements might be made in the future.

As the frequency and severity of droughts intensify, understanding how high yields can be maintained while increasing the WUE of crops will be necessary. Drought stress can significantly affect plant productivity and performance during growth and development (Reddy et al., 2004). The negative effects resulting from drought stress can be alleviated by drought stress tolerance or stress avoidance (Leakey et al., 2019). Drought tolerant plants use various mechanisms to continue metabolic functions in extreme drought environments. Plants can avoid drought stress by increasing their WUE. Increases in WUE can be achieved by reducing water use under favorable conditions, which maintains soil moisture for periods of drought. Because drought tolerance and avoidance are traits that remain different in their functions, and are likely mechanistically distinct, there is an opportunity to combine these traits to greatly improve yield under drought.

The identification of variation in WUE across diverse *Z. mays* lines has allowed for the development of WUE lines by some breeding programs. This has been accomplished through various methods such as transgenic approaches specifically targeting traits such as WUE in the case of Monsanto's DroughtGard hybrids. A set of non-transgenic Pioneer AQUAmax hybrids were shown to have significantly higher WUE and yields under drought environments compared to control hybrids (Hao et al., 2015). Interestingly, these conventional lines were selected using managed drought environment trials, which demonstrates that selection for drought tolerance can successfully increase WUE through different traits. However, as previously mentioned, a lack of high throughput methods to identify WUE lines has limited the ability to specifically breed for increases in WUE. This is especially true for WUE under well-watered conditions.

Current climate projections support the need to improve water use in major crops; however, we need to be cognizant of whole plant effects resulting from increasing TE. Although there are

obvious benefits to improving WUE by reducing transpiration, there are also some potential drawbacks. While selecting for increases in WUE, it is important to make sure yield is not negatively impacted. When WUE values are high, decreases in intercellular CO_2 levels (C_i) can occur (Blum, 2009). If g_s is modified to decrease transpiration rates, sufficient C_i values need to be maintained to provide CO_2 flux through the photosynthetic pathway. To visualize the importance of WUE for yield, we look at Passioura's yield equation.

$$\text{Yield} = T * WUE * HI$$

As shown above, yield is the product of transpiration rates (T), WUE, and harvest index (HI). Due to the correlation between C_i and A, increases in A would result in a drawdown of CO_2 and lower C_i/C_a values. This C_i/C_a reduction would result in increased WUE if g_s does not also increase as a result. Specifically in C_4 plants, there is potential to increase WUE while maintaining necessary CO_2 concentrations around Rubisco in bundle sheath cells. A high C_{bs}/C_i ratio is achieved in C_4 plants through the use of the carbon concentrating mechanism, therefore there is potential that high A rates could be maintained under low g_s levels (Leakey et al., 2019). As a result, C_4 plants can operate at a lower C_i, allowing potential improvements in WUE without any negative yield loss. Thus, it is important to understand the whole plant and WUE interaction to work towards maintaining or increasing productivity and yield while selecting for high WUE.

The use of $\delta^{13}C$ as a proxy trait could significantly aid in the high throughput identification of TE lines across diverse germplasm resources. While $\delta^{13}C$ could be used to identify lines with high TE, it does not always aid in the identification of high yielding lines, or even WUE lines. It is important to understand that $\delta^{13}C$ is a per unit area measurement used as a proxy trait to quantify TE, and not a measurement of whole-plant WUE. Transpiration efficiency is one of a set of factors that determine whole plant WUE. Therefore, stable carbon isotope analysis is not solely an identifier of elite germplasm, but rather a tool that can be integrated into a set of breeding practices to identify material with high WUE that also maintain productivity.

Improvements in plant WUE have also been achieved by identifying and manipulating regulators of plant architecture and leaf morphology (Leakey et al., 2019). In addition to genetic variation, the regulation of genes controlling stomatal development and g_s have been investigated using a biotechnology approach to improve WUE. In rice, decreasing stomatal density was shown to

conserve water and improve drought tolerance (Caine et al., 2019). In our work, we identified genes responsible for stomatal response to changing atmospheric CO_2 concentrations. We were able to identify mutants that are insensitive to high CO_2 concentrations. Although maintaining high g_s levels under high CO_2 concentrations does not improve WUE, these finding can still be beneficial to the production of a more WUE *Z. mays* lines. Through the characterization and identification of genes important to stomatal signaling, we can begin to understand the mechanistic pathways controlling stomatal response. With a complete understanding of the signaling pathways, we can begin to engineer stomatal dynamics for the production of high yielding and WUE crops that are resilient to climate change.

Future investigation of the CO_2 stomatal signaling pathway in *Z. mays* will include targeting the paralogs of genes characterized in this study. As previously discussed, due to the recent whole genome duplication in *Z. mays*, it frequently contains gene copies that can serve redundant functions or occasionally become sub functionalized. In some cases, we were not able to see a stomatal response phenotype while targeting one or even two gene copies. Therefore, targeting additional gene copies and producing higher order mutants will aid it determining their role in stomatal response to changing CO_2 levels. Transposon mutants are desirable as they are non-regulated and available for public use upon request. They are also an affordable and timely alternative to the production of transgenic lines. However, because there are no available mutant stocks containing transposable element insertions in the untargeted gene copies, directed transgenic approaches will be necessary. Currently we are generating additional mutants using RNAi constructs.

As the weather during the growing season becomes less predictable and more extreme due to climate change, it will be necessary to combine approaches to develop resilient crops. Using $\delta^{13}C$ as a method to quantify TE and integrating this information into breeding programs will aid in the preservation of available fresh water. Through the genetic control of genes regulating stomatal movement, stomatal dynamics can be engineered to respond efficiently to environmental changes and maintain efficient transpiration rates. Although natural variation can be used to optimize crop efficiency, breeding and biotechnology approaches will both contribute to the production of WUE crops. Some mechanistic control that has the potential to increase crop efficiency is not attainable with natural variation. Due to the difference between agricultural and

natural systems, sometimes the desired trait cannot be found by screening diversity panels. In addition, the changes in our climate that we are experiencing are occurring at a rate much faster than that of evolution. Therefore, in cropping systems, biotechnology may be necessary to supplement traditional evolution and natural selection. The severity of our situation will require us to bring to bear both breeding and biotechnology methods if we aim to succeed in producing crops to feed our growing population.

REFERENCES

Blum, A. (2009). Effective use of water (EUW) and not water-use efficiency (WUE) is the target of crop yield improvement under drought stress. *Field crops research*, *112*(2-3), 119-123.

Caine, R. S., Yin, X., Sloan, J., Harrison, E. L., Mohammed, U., Fulton, T., Biswal, A., Dionora, J., Chater, C., Coe, R., Bandyopadhyay, A., Murchie, E., Swarup, R., Quick, & W., Gray, J. & Bandyopadhyay, A. (2019). Rice with reduced stomatal density conserves water and has improved drought tolerance under future climate conditions. *New Phytologist*, *221*(1), 371-384.

Hao, B., Xue, Q., Marek, T. H., Jessup, K. E., Becker, J., Hou, X., Xu, W., Bynum, E., Bean, B., Colaizzi, P., & Howell, T. A. (2015). Water use and grain yield in drought-tolerant corn in the Texas High Plains. *Agronomy Journal*, *107*(5), 1922-1930.

Leakey, A. D., Ferguson, J. N., Pignon, C. P., Wu, A., Jin, Z., Hammer, G. L., & Lobell, D. B. (2019). Water use efficiency as a constraint and target for improving the resilience and productivity of C3 and C4 crops. *Annual review of plant biology*, *70*, 781-808.

Reddy, A. R., Chaitanya, K. V., & Vivekanandan, M. (2004). Drought-induced responses of photosynthesis and antioxidant metabolism in higher plants. *Journal of plant physiology*, *161*(11), 1189-1202.

APPENDIX A

Supplemental Figures and Table

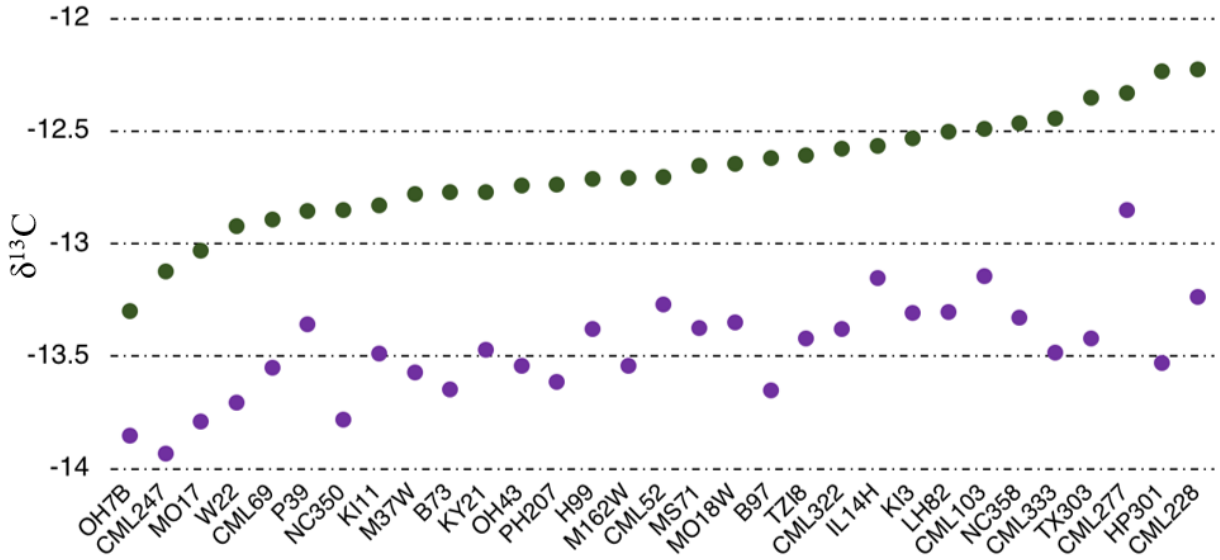

Figure A.1: Juvenile and adult leaf $\delta^{13}C$ among diverse *Z. mays* lines.

Data points represent $\delta^{13}C$ values from pooled samples of juvenile (purple) and adult (green) leaves for 31 *Z. mays* lines.

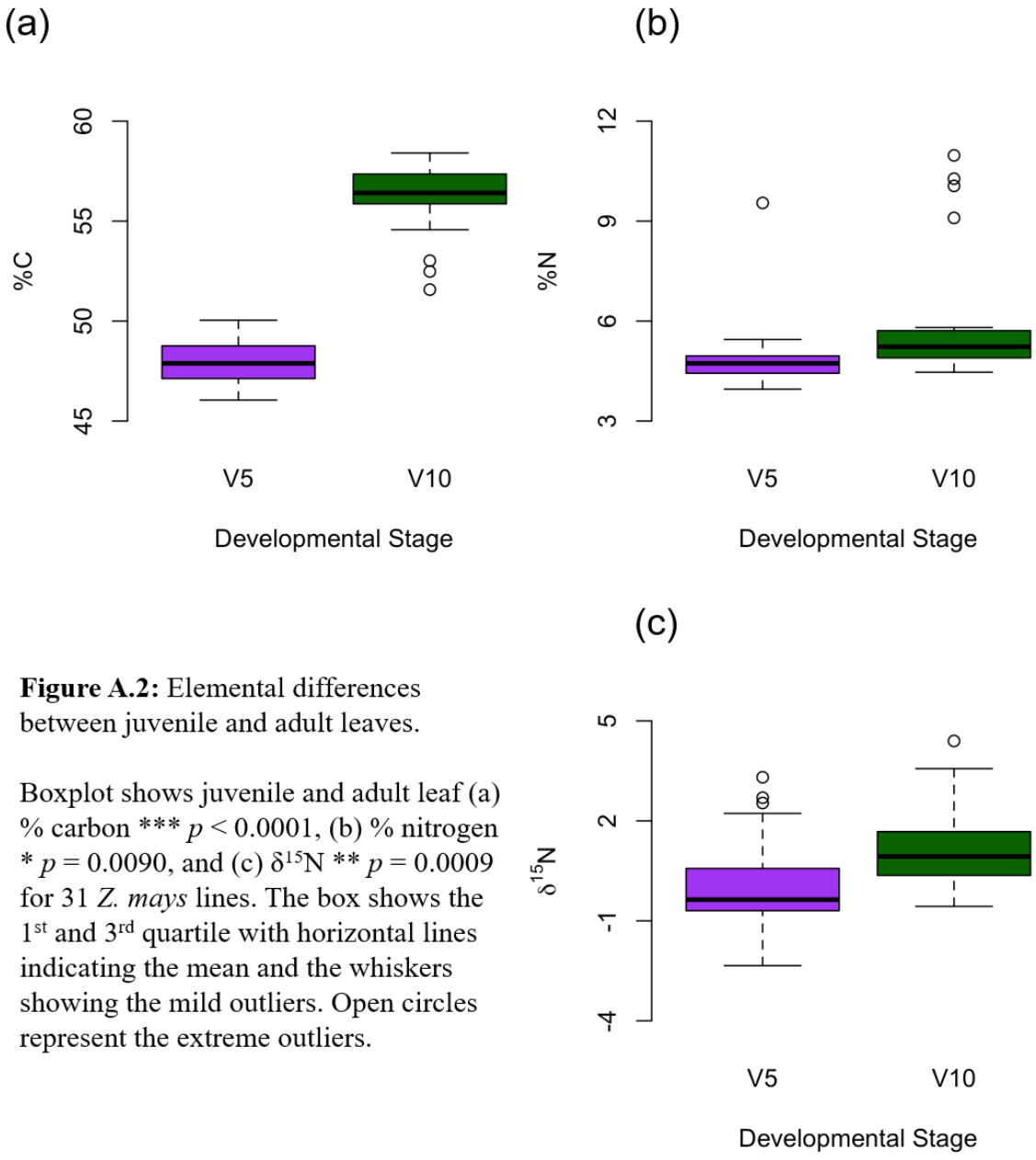

Figure A.2: Elemental differences between juvenile and adult leaves.

Boxplot shows juvenile and adult leaf (a) % carbon *** $p < 0.0001$, (b) % nitrogen * $p = 0.0090$, and (c) $\delta^{15}N$ ** $p = 0.0009$ for 31 *Z. mays* lines. The box shows the 1st and 3rd quartile with horizontal lines indicating the mean and the whiskers showing the mild outliers. Open circles represent the extreme outliers.

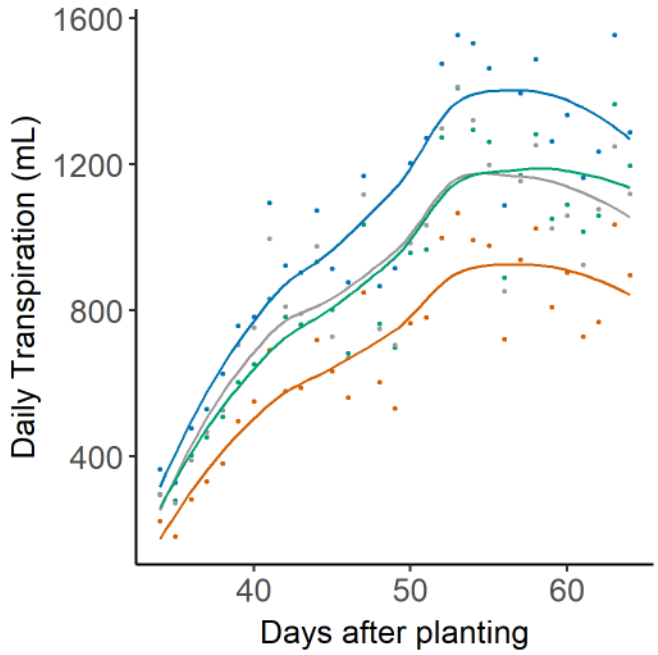

Figure A.3: Daily transpiration of four greenhouse grown *Z. mays* RILs.

Total water used daily over 32 days of water treatment. Gray (Z021E0032), orange (Z007E0150), green (Z021E0097), and blue (Z007E0067) points represent means of each RILs grown in the 100% FC treatment.

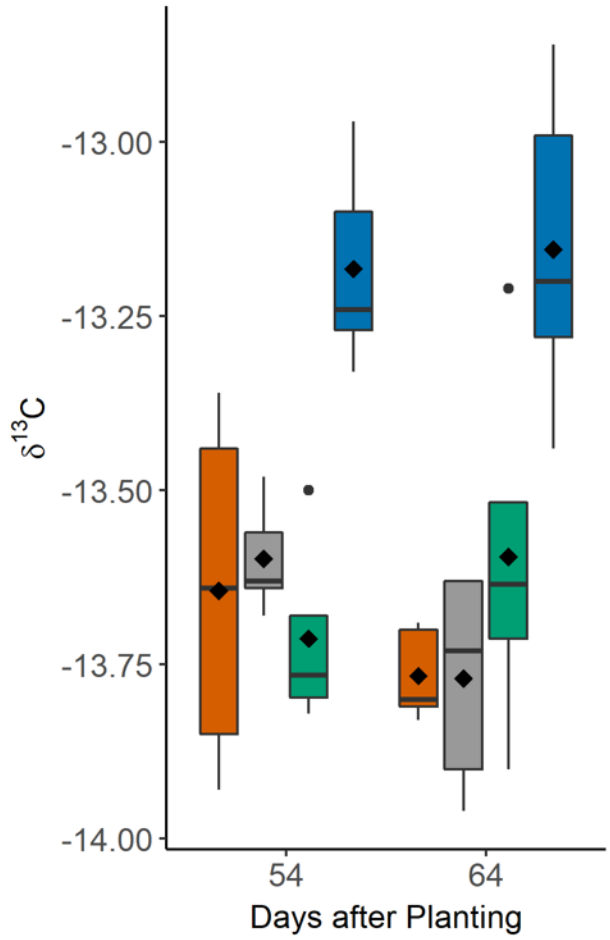

Figure A.4: Leaf $\delta^{13}C$ from 100% FC treatment collected 54 and 64 day after planting.

Boxes show the first, second, and third quartiles. The diamond represents the mean. Whiskers represent minimum and maximum observations. No significant differences were found between the two collection times.

Table A.1 Leaf $\delta^{13}C$ of diverse *Z. mays* inbred lines.

Line	2015 $\delta^{13}C$	2015 Rank	2016 $\delta^{13}C$	2016 Rank	Average Rank
HP301	-11.65	3	-12.23	2	3
TX303	-11.87	4	-12.34	4	4
LH82	-11.61	1	-12.50	8	5
CML103	-11.64	2	-12.48	7	5
CML228	-11.99	8	-12.22	1	5
CML277	-11.99	9	-12.32	3	6
CML333	-12.00	10	-12.44	5	8
CML322	-11.92	6	-12.57	11	9
KI3	-12.09	12	-12.52	9	11
NC358	-12.16	18	-12.46	6	12
IL14H	-12.14	17	-12.56	10	14
B97	-12.12	15	-12.61	13	14
MS71	-12.12	14	-12.64	15	15
PH207	-12.04	11	-12.73	19	15
MO18W	-12.13	16	-12.64	14	15
P39	-11.88	5	-12.85	26	16
OH43	-12.12	13	-12.73	20	17
CML69	-11.96	7	-12.88	27	17
H99	-12.18	19	-12.70	18	19
TZI8	-12.27	25	-12.60	12	19
M162W	-12.21	21	-12.70	17	19
CML52	-12.34	26	-12.70	16	21
KI11	-12.20	20	-12.82	24	22
B73	-12.25	22	-12.76	22	22
M37W	-12.27	23	-12.77	23	23
NC350	-12.27	24	-12.85	25	25
KY21	-12.44	28	-12.76	21	25
OH7B	-12.44	27	-13.29	31	29
MO17	-12.47	29	-13.02	29	29
W22	-12.57	30	-12.92	28	29
CML247	-13.02	31	-13.12	30	31